LIMITING THE FAULT CURRENT OF A WIND TURBINE DRIVEN DOUBLY FED INDUCTION GENERATOR SYSTEM USING FUZZY RESISTANCE LIMITER.

By

Sudeep Thapaliya
20261009

A thesis submitted to the Department of Electrical and Electronic Engineering in partial fulfillment of the requirements for the degree of
Master of Science in Electrical and Electronic Engineering (M.Sc. in EEE)

Department of Electrical and Electronic Engineering
Brac University
August 2022

Declaration

It is hereby declared that

1. The thesis submitted is my own original work while completing degree at Brac University.
2. The thesis does not contain material previously published or written by a third party, except where this is appropriately cited through full and accurate referencing.
3. The thesis does not contain material which has been accepted, or submitted, for any other degree or diploma at a university or other institution.
4. I have acknowledged all main sources of help.

Student's Full Name & Signature:

Sudeep Thapaliya
20261009

Approval

The thesis titled "Limiting the fault current of a wind turbine driven doubly fed induction generator system using fuzzy resistance limiter" submitted by

Sudeep Thapaliya (20261009)

of Fall, 2020 has been accepted as satisfactory in partial fulfillment of the requirements for the degree of Master of Science in Electrical and Electronic Engineering on 14th August 2022.

Examining Committee:

Supervisor:
(Member)

____

Dr. Abu Hamed M. Abdur Rahim
Professor, Electrical and Electronic Engineering
Brac University

Internal Examiner:
(Member)

____

Dr. Shahidul Islam Khan
Professor, Electrical and Electronic Engineering
Brac University

External Examiner:
(Member)

____

Dr. Md. Quamrul Ahsan
Distinguished Professor, Electrical and Electronic Engineering
Green University of Bangladesh

Committee Chair:

____

Dr. Md. Mosaddequr Rahman
Professor and Chairperson, Electrical and Electronic Engineering
Brac University

Ethics Statement

This is to certify that this thesis titled "LIMITING THE FAULT CURRENT OF A WIND TURBINE DRIVEN DOUBLY FED INDUCTION GENERATOR SYSTEM USING FUZZY RESISTANCE LIMITER " is the result of my study for partial fulfillment of Master of Science in Electrical and Electronic Engineering degree under supervision of Dr. Abu Hamed M. Abdur Rahim, Professor, Department of Electrical and Electronic Engineering, Brac University and no part of this work has been submitted elsewhere partially or fully for the award of any other degree or diploma.

Abstract

A doubly fed induction generator (DFIG) is preferred over other wind generators because of its capacity to adapt to variable wind speeds and economic converter. DFIG is sensitive to grid faults as its stator is directly connected to the grid. To fulfill the grid code requirement, DFIG is required to be connected to the grid during the fault. Converter control is not sufficient to maintain grid stability. Ladder resistive fault current limiter (LRFCL) and fuzzy logic control-based series dynamic braking resistor (FLC-SDBR) are proposed for low voltage ride-through (LVRT) enhancement. The series resistor consumes the surplus active power during the grid voltage dip. A control system has been developed to control the step resistance in the LRFCL, whose operation changes with the deviation in grid voltage. A fuzzy logic-based control system has been developed to precisely control the power being consumed in the SDBR. The LVRT capability of the DFIG has been investigated for different levels of fault in bus terminals. The performance of the proposed model is compared with that of a resistive superconducting fault current limiter (R-SFCL) and a conventionally controlled SDBR. Simulation results performed in MATLAB show that the proposed model has the capacity to enhance LVRT for different levels of bus voltage sag. FLC-SDBR is superior in performance with a quick restoration of the system stability.

Keywords: DFIG, LVRT, SDBR, RSFCL, LRFCL, FLC-SDBR

Dedication

I dedicate my thesis work to my family and friends, who have always been a huge source of love, support and encouragement in my life.

Acknowledgement

I would like to express my sincere gratitude to my supervisor, Dr. Abu Hamed M. Abdur Rahim, Professor, Department of Electrical and Electronic Engineering (EEE) of Brac University for his insightful suggestions and comments for completing my M.Sc. in EEE thesis work.

I would also like to thank the Dean of School of Engineering, Brac University, the Chairperson, Department of EEE, Brac University and the Program Coordinator, Post Graduate Program, Department of EEE, Brac University for their co-operation. I acknowledge the facilities and support provided by the Brac University for completing my thesis work.

Contents

List of Tables

List of Figures

List of Acronyms

WECS	Wind Energy Conversion System
WT	Wind Turbine
HAWT	Horizontal Axis Wind Turbine
VAWT	Vertical Axis Wind Turbine
SCIG	Squirrel Cage Induction Generator
PMSG	Permanent Magnet Synchronous Generator
DFIG	Doubly Fed Induction Generator
RSC	Rotor Side Converter
GSC	Grid Side Converter
MPPT	Maximum Power Point Tracking
LVRT	Low Voltage Ride Through
HVRT	High Voltage Ride Through
FCL	Fault Current Limiter
ANFIS	Adaptive Network-Based Fuzzy Inference System
SMES	Superconducting Magnetic Energy Storage System
SC	Superconducting Coil
ESD	Energy Storage Device
ESC	Energy Storage Side Converter

BESS	Battery Energy Storage System
SFCL	Superconducting Fault Current Limiter
N-SFCL	Non-Superconducting Fault Current Limiter
CB-SFCL	Capacitive Bridge Type Superconducting Fault Current Limiter
MBR-SFCL	Modified Bridge Resistive Superconducting Fault Current Limiter
BFCL	Bridge Fault Current Limiter
CB-FCL	Capacitive Bridge Fault Current Limiter
MBFCL	Modified Bridge Fault Current Limiter
NC-MBFCL	Non-Linear Controlled Modified Bridge Fault Current Limiter
PRFCL	Parallel Resonance Bridge Fault Current Limiter
LRFCL	Ladder Resistive Fault Current Limiter
SDBR	Series Dynamic Braking Resistor
FLC-SDBR	Fuzzy Logic Control Series Dynamic Braking Resistor
R-SFCL	Resistive-Superconducting Fault Current Limiter
FCL	Fault Current Limiter
PWM	Pulse Width Modulation
MF	Membership Function
FLC	Fuzzy Logic Control

List of Symbols

P_m	Turbine power output
V_w	Wind speed
β	Blade pitch angle
λ	Tip speed ratio
A	Area swept by turbine blade
R_s	Stator resistance
x_s	Stator reactance
x_m	Stator-rotor mutual reactance
R_r	Rotor resistance
x_r	Rotor reactance
R_a	Stator side converter resistance
X_a	Stator side converter reactance
C	Converter capacitance
Vc	Converter DC-link voltage
R	Transmission line resistance
X	Transmission line reactance
$m1, m2$	Modulation index of grid and rotor side converter
$\alpha 1, \alpha 2$	Phase angle of grid and rotor side converter

i_{sd}, i_{sq}	d-q axes stator current
i_{rd}, i_{rq}	d-q axes rotor current
v_{sd}, v_{sq}	d-q axes stator voltage
v_{rd}, v_{rq}	d-q axes rotor voltage
i_{ad}, i_{aq}	d-q axes converter current
ω_s	Stator frequency
ω_r	Rotor frequency
ω_0	Base angular frequency

Chapter 1

Introduction

1.1 Background

With the advancement in technology and rapid industrialization, electricity demand is increasing all over the world. Electricity has been an essential part of human life. It is impossible to imagine a modern society without electricity. Conventional energy sources like coal, diesel, and gas are polluting the air with the emission of carbon dioxide and greenhouse gases. Non-renewable sources of fuel are the primary cause of global warming, leading to problems like melting of glaciers, heat waves, rising sea levels, etc. With environmental concerns and the inadequacy of fossil fuels in the near future, the whole world is focusing on renewable generation sources. Renewable energy sources like solar energy, hydropower, wind and tidal energy are clean and green sources of energy. Wind energy is gaining popularity as a clean and economical source of energy production. As a result, wind energy's contribution to the overall energy market is growing. In 2020, electricity generation from wind increased by almost 170 TWh (+11%). 108 GW of onshore and 6 GW of offshore wind energy were added in 2020. To meet the net-zero power generation level by 2050, 8000 TWh of wind power should be installed with net growth of 18% per year [1].

The EU has the largest floating (offshore) wind power capacity, i.e., 70% of the total worldwide. It is predicted that by 2030, wind energy capacity installations will reach 350 GW, supplying up to 24% of electricity demand [2]. Europe is leading in the wind power production sector [3]. China and USA are leading the wind power generation industry with 55.91% and 18.19% of the total production of 93 GW worldwide [4].

1.2 Wind Turbine Generator System Components

A wind energy conversion system (WECS) is the system of converting the kinetic energy present in the wind to mechanical energy through a wind turbine, which is finally converted into electrical energy with the help of a generator. The wind turbine (WT) comprises blades, a rotor hub, and a nacelle [5]. The drive train consists of a low-speed shaft, a gearbox, and a high-speed shaft. A low-speed shaft is connected to the rotor blade. The torque generated by the low-speed shaft is transferred to a high-speed shaft connected to the generator, which rotates the generator rotor at high speed to produce electricity. An anemometer senses the wind speed and a wind vane senses the direction of wind flow. The control system senses those signals and provides a command to the yaw motor to rotate the rotor blade towards the direction of airflow for maximum power generation.

The brake is placed in the high-speed shaft so that the brake can be applied to the rotor during the aerodynamic failure and hold the rotor in standstill conditions. The pitch angle of the rotor blade is controlled for maximum power. Usually, the power produced is at low voltage, so the generated power is transferred to the transformer or substation at the foot of the tower. Then the voltage is stepped-up and fed to the transmission or distribution line. The cooling system is provided to cool the generator and the braking system. An electric fan or oil cooling mechanism is used for cooling purposes.

1.2.1 Wind Turbine Types

Based on physical structure, wind turbines can be classified as [6]:

a) Horizontal axis wind turbine (HAWT)

In HAWT, the rotational axis is parallel to the ground. The HAWT is a large turbine being used for harnessing more wind energy. The efficiency of this type of turbine is about 50–60%. The HAWT is further classified as:

i) Upwind HAWT

In this type of wind turbine, the wind will hit the blade which is in front of the tower [7]. A yaw mechanism is necessary for the proper orientation of a wind turbine. Upwind HAWTs are widely used in the United States of America.

ii) Downwind HAWT

In this HAWT, the wind will strike the tower head then only to the blade. It can work well without using the Yaw mechanism, which is made possible with the advanced design of the nacelle and rotor.

HAWT can have a different number of blades. The efficiency of HAWT along with its blade is as shown in the table below:

Number of blades	Efficiency (%)
1	43
2	47
3	50

b) Vertical axis wind turbine (VAWT)

VAWT has a rotational axis perpendicular to the ground [8]. They are being used for residential applications and small wind farms. The efficiency of this type of turbine is more than 70%. The various kinds of VAWT are:

i. Savonius

ii. Darrieus-rotor

iii. H-Darrieus

iv. Helix shape

The comparative analysis of HAWT and VAWT are shown below:

HAWT	VAWT
Wind flowing directly to the blade surface is used for power generation.	Wind flowing from any direction is used for power generation.
HAWT is more economical.	VAWT is less economical but portable.
Machinery is placed at top of the tower.	Machinery is placed at the base of the tower.
A yaw mechanism is needed to move the blade towards the direction of air flows.	No need of a yaw mechanism as airflow from any direction will contribute to power generation.
Once the wind speed reaches above the cut-in speed, turbine will start automatically.	Initial torque should be provided externally to start the turbine.

1.2.2 Wind Turbine Generators

The mechanical torque developed in the wind turbine is transferred to the generator rotor through the shaft for the power generation. Different types of generator schemes in the wind farm are discussed briefly [9]:

a) Squirrel Cage Induction Generator (SCIG)

SCIG shown in Fig 1. 1 is a popular and commonly used generator due to its simple design considerations. The wind turbine shaft is connected to the generator through the gearbox [10].

The variation in the rotor speed is minimal, due to which it is considered as the fixed speed wind turbine. SCIG can also be modified and used as a variable speed generator through a full-scale power electronic converter. But with the use of a full-scale converter, the cost of the overall system increases. There is no need for brushes for an advantageous operation. As compared to conventional synchronous generators, SCIG has advantages like simplicity in construction, low maintenance due to a brushless system and economical [11].

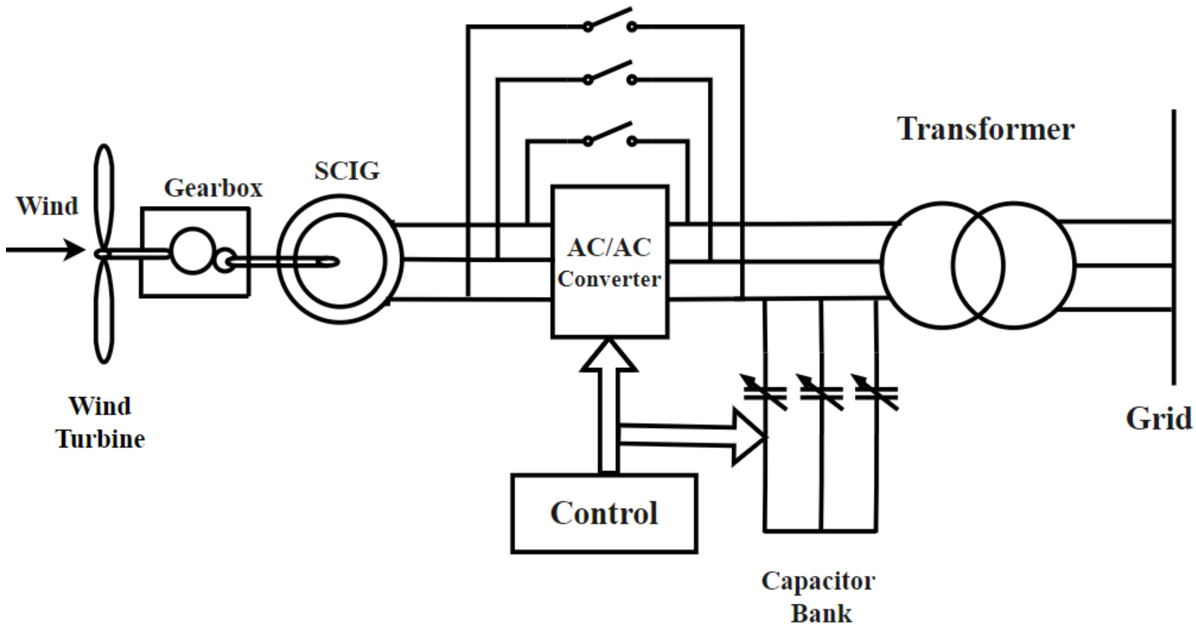

Fig 1. 1: Squirrel Cage Induction Generator

b) Permanent Magnet Synchronous Generator (PMSG)

Due to its simple structure and efficient power production, PMSG is used in large-scale power production [12]. A PMSG is a type of brushless synchronous generator in which field excitation is provided by a permanent magnet. The permanent magnet is placed in the rotor from which field excitation is produced without the need for an external supply. The stator of PMSG is connected to the grid through the back-to-back converter as shown in Fig 1. 2 [13]. With the variable wind speed, the voltage produced is of variable amplitude and frequency. Due to variation in voltage and frequency, the system cannot be connected directly to the grid. The AC-DC-AC converter produces power with the desired frequency and voltage. Since the full range converter is required for the whole power conversion, it makes the overall implementation of the system costly.

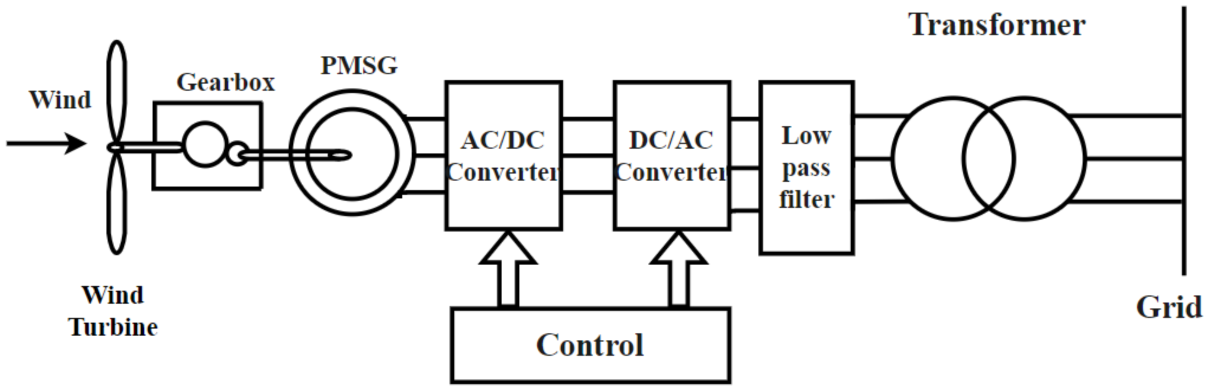

Fig 1. 2: Permanent Magnet Synchronous Generator

c) Doubly Fed Induction Generator (DFIG)

DFIG shown in Fig 1. 3, is the wound rotor induction generator. It is an advanced and widely used technology for wind power generation. The stator of the DFIG is directly connected to the grid, so synchronization is most important. While the rotor is connected through the back-to-back converter. The voltage and frequency of the rotor circuit are varied through the converter control to produce the output power with the desired frequency and voltage from the stator. The rotor side converter (RSC) is responsible for controlling the active and reactive power while the grid side converter (GSC) maintains DC-link voltage [14]. Since only 25–30% of total power flows through the rotor, the converter size is reduced, which makes the system more economical to implement. The reduced cost of the inverter filter helps to make the system more economical and advantageous. It can work with a 33% margin in synchronous speed, so it has high flexibility in speed variation [15]. The stator is directly connected to the grid, which makes the system highly sensitive to grid faults and disturbance [16].

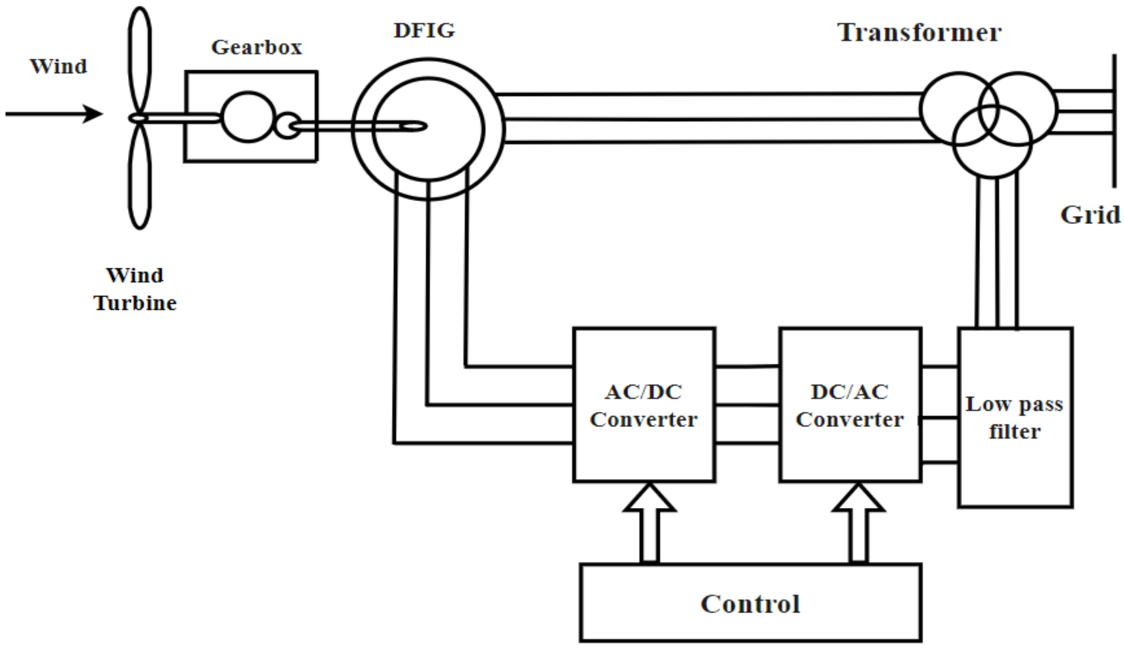

Fig 1. 3: Doubly Fed Induction Generator

1.3 Power Curve Characteristics of wind turbine

Wind speed varies every second. Low wind speed may not have sufficient energy or torque to rotate the rotor, while high wind speed may damage the turbine due to mechanical failure. Based on wind speed, the operation ranges of wind turbines can be divided into three different operating stages, shown in the power curve (Fig 1. 4) [17]. Cut-in speed is defined as the minimum wind speed required for a wind turbine for the power generation process to start, which is usually around 4 m/sec. Below the cut-in speed, wind turbine remains idle. Rated speed is the speed at which the wind turbine will generate rated power. In between the cut-in speed and the rated speed, the blade of wind turbines is pitched into the wind speed with an optimal angle of attack. Maximum power point tracking (MPPT) is activated to generate the maximum power from the corresponding wind speed. With the operation of MPPT, turbine rotational speed is varied to track the maximum power at different wind speeds. Above the rated speed, blade pitch control will be activated. With the help of the pitch control mechanism, the captured power is kept constant. Only the power equivalent to the rated power of the wind turbine generator is captured. With increased wind speed, the rotor blades are pitched out of the wind and generator speed is maintained. Thus, pitch control helps to control the aerodynamic torque applied to the rotor blade.

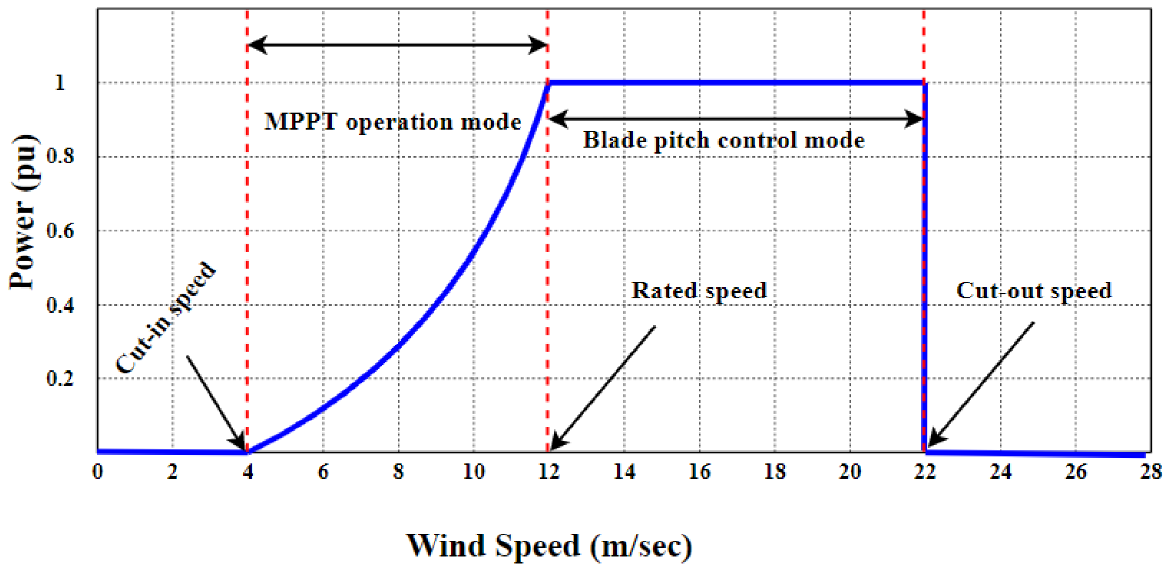

Fig 1. 4: Power curve of variable speed wind turbine

At very high speeds (above 22 m/s), huge pressure will be generated in the blade leading to mechanical failure. The wind turbine is shut down by applying a mechanical brake when the wind speed rises above the cut-out speed. Once the wind speed returns to a safe value (i.e., wind speed between 4 m/s and 22 m/s), the mechanical brake is released, and the wind turbine starts generating power.

1.4 Grid Code

A grid code requirement suggests that a wind farm needs to be connected to the grid for a certain time as specified by the grid operator to support the grid voltage during the disturbance or fault. In the past, when the wind power penetration into the power system was low, there was no strict grid code for the wind farms. Wind turbines or farms used to supply only a small percentage of overall power, so they were allowed to shut down during the grid fault. Since the power provided weightage was low, it did not affect the system stability. In the present scenario, with the advancement in wind power technologies, wind power contribution has increased in the grid. In case of high penetration, the wind farms are not allowed to shut down during the grid disturbances to avoid system collapse and resulting blackout.

Power system characteristics are diverse in different countries, so grid code requirement changes from one grid operator to another. The common and major requirements for the connection of wind farms to the grid for a typical grid code are as follows [18]:

a) Voltage variation range

The wind farm should fulfill the voltage requirement and should be connected to the grid for the specified time period. For both low voltage ride through (LVRT) and high voltage ride through (HVRT) wind farm is needed to be in continuous operation until the shut time as allowed by the grid operator.

b) Frequency range

The wind farm is required to operate during a certain frequency deviation. The wind farm should be in continuous operation for a frequency range of 49.8 Hz to 50.2 Hz. For the frequency range of 47.5 Hz to 52 Hz, it should be in connection for 60 seconds. Mandatory connection time reduces to 20 seconds for the frequency range of 47 Hz to 47.5 Hz [19]. This range varies from country to country and also from operator to operator.

c) Active and reactive power

Wind farms need to supply the required active power to support the stable frequency in the system. Some grid code suggests supplying the reactive power to maintain the grid voltage and power factor during fault. The grid code requirement varies from time to time. With an increase in the wind power penetration, it gets stricter which can be understood from the change in grid code requirement of the German power grid from 2004 to 2016, shown in Fig 1. 5 [20].

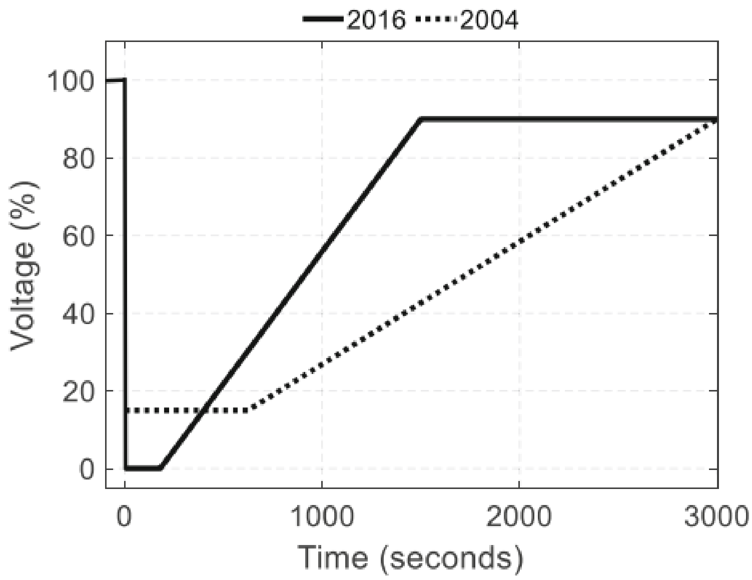

Fig 1. 5: The change in grid code requirement in German from 2004 to 2016

1.5 Controls to Ride Low Voltage

WECS is a reliable option to tackle global environmental issues as wind energy is available everywhere day and night. Though this system has a positive impact from an ecological point of view, several technical problems need to be addressed for the sustainable growth of the wind power generation system. In the past, there was not much wind power penetration in the grid. But now, with the advancement in technology, its impact has drastically increased in the last decades. Numerous challenges have been set in the power system as wind energy flow cannot be predicted as wind speed varies from time to time.

Among different wind turbine generators, DFIG is gaining popularity and is widely being used. During regular operation, pitch control [21] and MPPT [22], along with some converter control strategies, are sufficient to deal with the changing wind speed and deviation in power. The real challenge is during the fault. DFIG is more vulnerable to a grid fault and transmission line network disturbance. A voltage dip in the bus terminal will directly affect the generator's terminal voltage. With a voltage dip, a large amount of current will flow through the stator and rotor, which can damage the converter and rotor windings. If the DFIG is isolated from the grid, there will be a chance of blackout as the DFIG's power contribution to the system is high. DFIG should remain connected to the grid to increase the system's reliability. Surplus power during voltage sag should be consumed in dump load or stored in the energy storage devices.

Different control strategies are being used to sense the faulty condition in the DFIG. Those control circuits will enable the operation of the different auxiliary devices embedded for LVRT enhancement of DFIG. The various control strategies for switching the series compensating devices are:

a) Conventional control

In the conventional control scheme, a bypass switch or insulated-gate bipolar transistor (IGBT) switch is controlled by applying a high (1) or low (0) signal in the gate of the IGBT. Mostly system voltage or voltage at the point of common coupling (PCC) is compared with the threshold voltage and the control signal is generated [23]. When the voltage at PCC is less than the threshold voltage, it is considered as the condition of voltage sag. A low signal is sent to the gate of the IGBT, which will turn off the IGBT leading to the activation of the series compensating device. The conventional circuit with voltage as the control signal to generate the gate pulse for the IGBT is shown in Fig 1. 6 [24]. In some cases, DFIG active power output is compared with a threshold value to generate IGBT pulses [25].

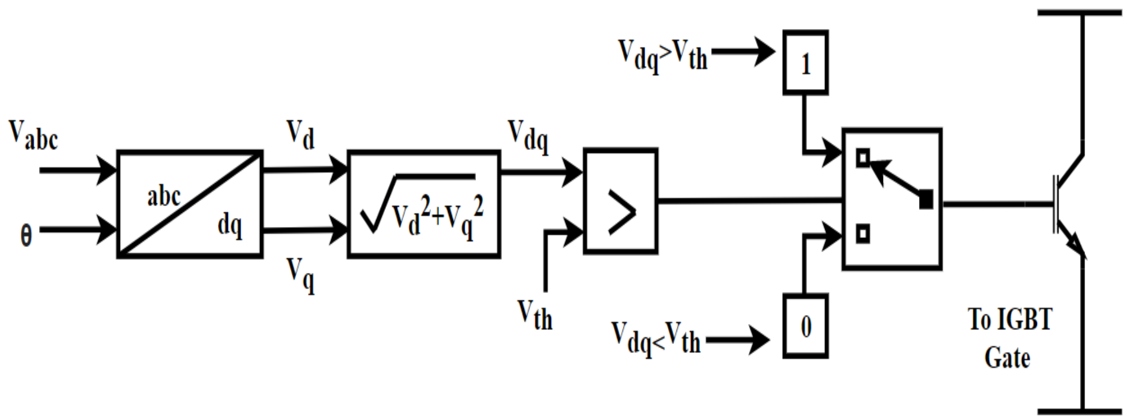

Fig 1. 6: Conventional controller based on single input

Current and voltage can be used as the reference for generating a control signal [26]. The control circuit is shown in Fig 1. 7 [27]. In this scheme, the current signal is used to detect the fault, and the voltage signal is used to detect the system voltage recovery with the elimination of the fault. Once the current rises above the threshold value, the fault is detected and IGBT is turned off. After the clearance of fault, voltage is recovered, which is sensed by the voltage comparator and the IGBT is turned on [28].

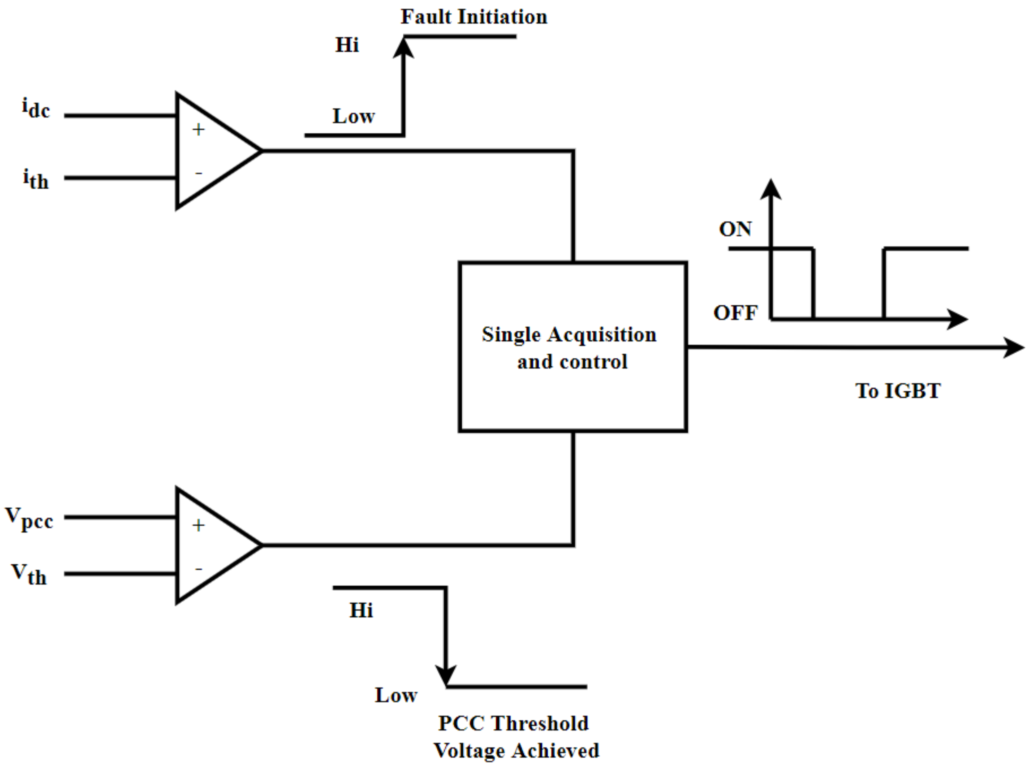

Fig 1. 7: Conventional controller based on multiple input

b) Non-linear feedback control

In this scheme non-linear equation is used to generate the duty cycle (d). The input of the non-linear control block is the voltage deviation (ΔV). Different papers propose different non-linear equations. The non-linear equation, as mentioned in the papers [29-30], is given as follows:

$$d = \log\left(1 + (k * \Delta V)\right) \tag{1.1}$$

$$d = 1 - e^{-k * \Delta V} \tag{1.2}$$

Here k is the constant whose optimum value is calculated by the trial method. The control circuit is shown in Fig 1. 8.

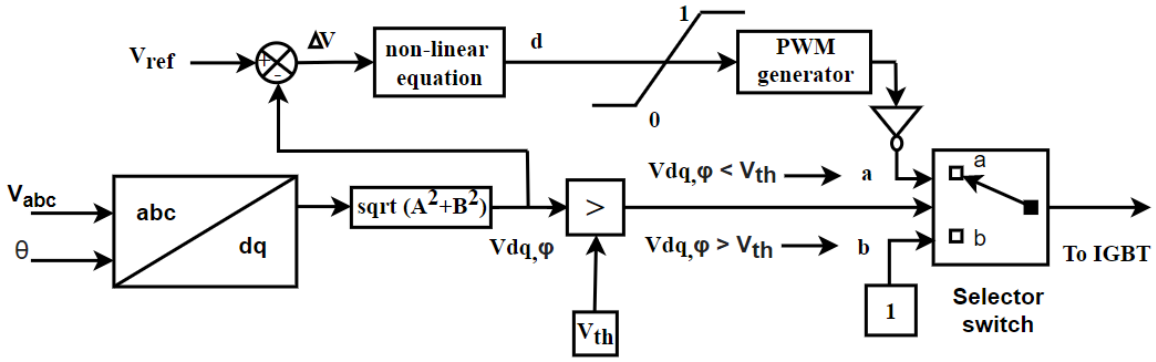

Fig 1. 8: PI based controller

When the system voltage falls below a certain threshold, the switch selector selects the switch 'a'. Pulse width modulation generator generates the pulse with respect to duty cycle to control power flowing to series compensating device. The equivalent impendence offered is d*z during the voltage sag. Z is the impedance of the series compensating device. During normal conditions, system voltage is higher than the threshold, so selector will select switch 'b'. This will turn on IGBT and a low resistance path is provided for power flow.

c) Proportional-integral (PI) based control

The control circuit of the PI-based controller is similar to that of a non-linear controller. The fundamental difference here is that PI control generates the duty cycle [31]. The optimal value of the proportional and integral gain is calculated and incorporated into the system.

d) Artificial intelligence-based control

In this scheme, different technologies like fuzzy and neuro fuzzy are used to generate the duty cycle for optimal control of the series compensating devices [32]. One or more of the system variables like current, voltage and rotor speed can be incorporated to generate the control signal as per the need of the system. The fuzzy-based control scheme is explained in detail in chapter 4.

Those control schemes are basically designed to work for the worst-case scenario of 0 dip in bus voltage. This control system does not consider the change in the control strategies with a change in level of voltage sag. For less voltage deviation also full resistance value is activated in the system. A control system has been proposed in this thesis work whose control strategies change with the change in voltage sag level. Ladder resistive fault current limiter (LRFCL) is proposed to enhance system stability for any level of voltage sag in the system. Also, a fuzzy logic-based control system is proposed to precisely control the series dynamic braking resistor (SDBR), whose control action changes from point-to-point deviation in voltage.

1.7 Objective of the Thesis

The objectives of this research are the following:

- To develop a DFIG model in MATLAB which is connected to the infinite bus through the transmission line.
- To develop a resistive fault current limiter that can work effectively for different levels and extents of voltage dips at the grid.
- Since the nature of the faults and disturbances are not known ahead of time, this thesis proposes to explore the design of a fuzzy-logic based control system for proper switching of the IGBT.
- To develop a control strategy for switching fault current limiters (FCL).
- To compare the proposed model with the existing technologies like conventional controller based SDBR and R-SFCL to verify the effectiveness of the proposed model.

1.8 Methodology

In order to achieve the objective of the thesis following methodology is used:

- DFIG and its converters (RSC and GSC) are developed through MATLAB programming.
- DFIG system model is connected to the infinite bus through a transmission line, which includes a local load at the machine terminal.
- Calculation of the required value of series resistance to absorb the excess power during the grid voltage dip.
- Time-varying mathematical modeling of the resistive type superconducting fault current limiter (R-SFCL) is developed for modeling.
- Control system with IGBT switching algorithm is developed for proper switching of IGBT switches in LRFCL.
- Fuzzy based control system is developed for precise control of the power being dropped in the series resistance, which is done with a variation of the controller output with deviation in bus voltage.
- For evaluation of transient stability, different levels of voltage dip are considered in the bus terminal.
- System responses such as rotor current, stator current, generator speed, stator terminal voltage and DC-link voltage along with output power are observed with and without FCLs.
- Deviation area of the system parameter from the steady state is calculated with the index-based calculations method.

1.9 Organization of the Thesis

The contents of the thesis are organized as follows:

Chapter 2: Literature review

Different kinds of technologies used for the LVRT enhancement of the DFIG are described in this chapter.

Chapter 3: System model

Mathematical modeling of DFIG along with its converter system is described in detail. Wind turbine and local load are modeled in this section.

Chapter 4: Fault current limiters modeling and control

This section explains different fault current limiters (FCLs) like SDBR, R-SFCL and LRFCL and their mathematical model. Also, the control system for correctly triggering the FCL during dip is mentioned. The fuzzy logic-based control system is developed for activating the IGBT switches.

Chapter 5: Simulation results

The results obtained from MATLAB using various fault current limiting techniques are compared in this section. Stator and rotor current, DC-link voltage, terminal voltage, output power and generator speed obtained from the different LVRT enhancement technique is plotted. The index-based calculation is performed.

Chapter 6: Conclusion and future work

The thesis work is summarized and concluded in this section. Also, the scope of the future work is presented.

Chapter 2

Literature Review

Different researchers have put forward solutions for LVRT enhancement of the DFIG. There are various hardware and software solutions for maintaining the system reliability. The software solution focuses on different control strategies, which are achieved through the controller schemes of the RSC and GSC converters. This research thesis is based on the hardware solution approach, so the literature review is mainly focuses on the hardware solution approach.

The hardware solution focuses on adding extra physical equipment with DFIG, which is activated during the disturbance or the fault in the system. The primary role of the hardware solution is to absorb the surplus power, i.e., the difference between the electrical power demand of the grid and the power produced by the wind generator. The hardware solution proposes the system with the combination of resistor, capacitor and inductor placed in a different location and unique orientation.

2.1 Crowbar

Crowbar is the traditional approach to the hardware solution of the LVRT enhancement of DFIG. The crowbar is positioned between the rotor windings and the RSC converter [33]. The rotor current is reduced during crowbar activation by adding the additional resistance in series with the rotor windings. At the same time, DFIG will absorb the reactive power from the grid as the RSC converter is turned off, making the DFIG function like the induction generator. This will cause the situation to deteriorate during the fault. [34] Reactive power demand exists in both the grid and the DFIG. Additional compensating equipment is required to supply the reactive power. An optimized switching crowbar method based on adjusting the time of the switching crowbar circuit is given to solve the problem [35]. The system may be unbalanced due to improper switching and an incorrect value of crowbar resistance. Crowbar resistance with a high value causes a rise in DC-link voltage, while a low value may not be enough to withstand the transient fault current. Furthermore, the transient cannot be handled effectively if the operating period is short. If the operating time is extended, DFIG will consume more reactive power. The criteria for selecting an acceptable crowbar reactance value and switching time are proposed [36]. It is determined that choosing the right crowbar reactance value and switching time can enhance LVRT for grid stability. However, the frequent switching of the crowbar circuit during dip has a distinct influence on the rotor circuit, which must be addressed in the future [37]. To support the dynamic reactive power, a new adaptive crowbar resistor has been developed [38].

2.2 Series Dynamic Braking Resistor

Crowbar activation leads to the operation of DFIG as an induction generator. To address the stated problem, SDBR has been proposed. During the grid fault, SDBR placed on the rotor side will be activated without causing the converter to shut down. SDBR resistance will consume surplus active power, contributing to system stability [39]. Maximum heat energy dissipation capacity and the temperature limit of the SDBR should be taken into consideration [40].

SDBR activation leads to a rise in the DC-link voltage. A hybrid model with the combination of DC-chopper is proposed [41] to maintain DC-link voltage. Compared to placement on the rotor side, SDBR placement on the stator side produces the best performance. When the system encounters a fault, a change in the voltage, current and speed is observed. It is verified that using the deviation of grid voltage to generate the switching signal provides a better response than using the variation of stator and rotor current [42].

2.3 DC-link Chopper

From the literature, it is known that the DC-link chopper is another prominent solution approach. The DC-link chopper is placed parallel with the DC-link capacitor. During the fault, there will be a power imbalance in the converter. Due to a decrease in terminal voltage, the converter fails to deliver the entire power to the grid. This leads to a rise in DC-link voltage. Thus, the chopper consumes excess power while maintaining the DC-link voltage [43]. A circuit diagram of the chopper, along with the generation of control signals, is shown in Fig 2. 1.

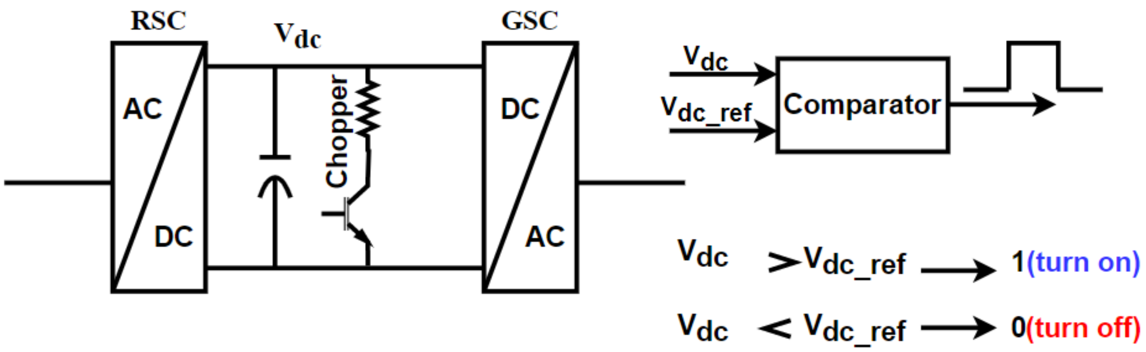

Fig 2. 1: DC-Chopper configuration with controller

Practical implementation of the DC-chopper and crowbar shows that the DC-chopper performs better [44]. If the chopper resistance is high, system performance will be decreased. It is suggested that for better performance, a chopper should be quickly inserted as soon as a fault is encountered in the system and the operation duration should be short. Chopper, along with SDBR implementation, is producing a better result [45]. A modified DC-chopper is proposed in the literature [46]. The control system is designed in such a way that the proposed system can be operated as a chopper or fault current limiter alternatively as per the system demand. An adaptive network fuzzy inference system (ANFIS) based control system for activating the chopper-crowbar protection scheme is proposed [47]. Stator side SFCL with the integration of a chopper is proposed. In this scheme [48], the chopper works as primary protection, limiting DC-link overvoltage. SFCL contributes to overcurrent protection.

2.4 Energy Storage System

Different sorts of energy storage-based protection schemes are proposed in the literature. The major role of energy storage is to store surplus power during the fault and return power after the clearance of the fault. A superconducting magnetic energy storage system (SMES) consists of superconducting coils (SC), which facilitate by balancing the variation in output power due to varying wind speeds during normal operating conditions. During a fault, SC limits the overcurrent [49].

Negative sequence stator current limiting overcurrent is countered by coordinated control of converters and energy storage devices (ESD). Also, reactive power is supplied simultaneously to support the terminal voltage after the clearance of a fault [50]. Increased rotor current is distributed between the RSC and the energy storage side converter (ESC), protecting the converters from overcurrent [51]. The different techniques described in the literature for storage systems include cooperative control of rotor side SMES and transient control [52], coordination of active crowbar with battery energy storage system (BESS) [53], and flywheel as energy storage [54].

2.5 Superconducting Fault Current Limiter

The other techniques used for the LVRT enhancement techniques of DFIG are the superconducting FCL (SFCL) and non-superconducting FCL (N-SFCL). SFCL (Fig 2. 2) possesses the superconducting state (negligible resistance) during normal conditions and high resistance during the fault. SFCL operation does not require any control action as SFCL comes into action once temperature, current density, or magnetic field rise above a particular threshold value [55].

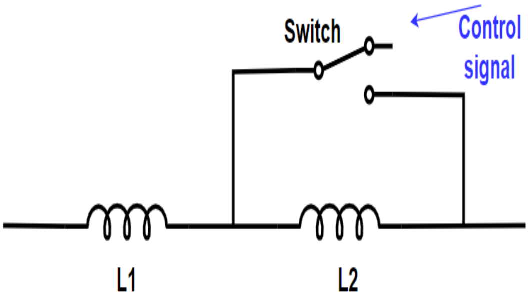

a) Inductive SFCL configuration

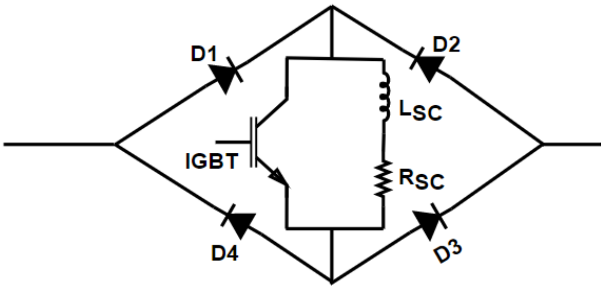

b) MBR-SFCL configuration

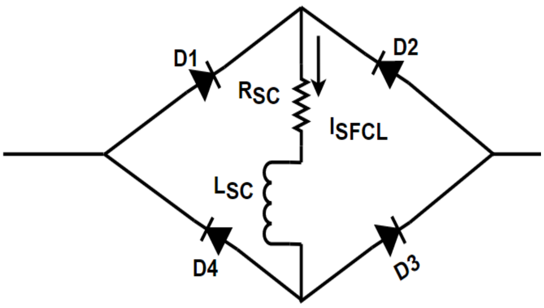

c) DC-resistive SFCL configuration

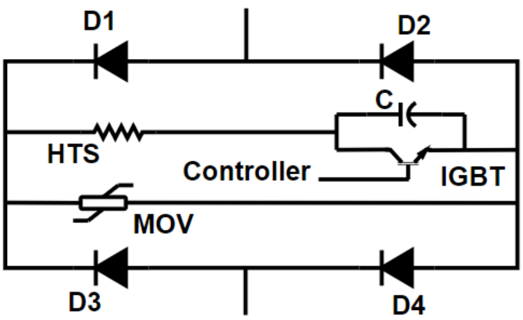

d) CB-SFCL configuration

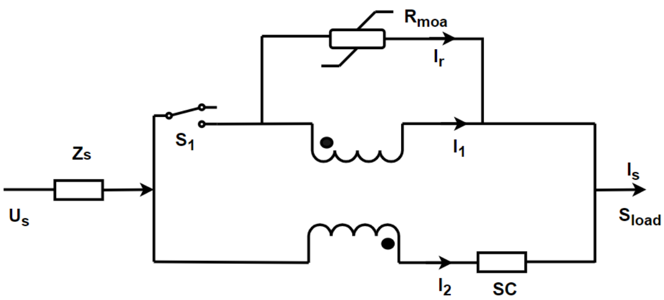

e) Flux-coupling SFCL configuration

Fig 2. 2: Configuration diagrams of SFCL

Resistive SFCL placed at the rotor side limits the rotor overcurrent during both symmetrical and unsymmetrical faults [56]. Inductive SFCL [57] plays the role of a filter during normal conditions. During fault demagnetization technique will limit overcurrent. Comparative analysis shows that resistive SFCL is superior to inductive in terms of current limiting ratio and restraining capacity [58].

The DC-resistive SFCL reduces the ac-loss in the superconductor using the diode bridge network. Due to self-quenching and self-recovery characteristics, a control system is not needed for activating the SFCL [59]. The capacitor bridge type SFCL (CB-SFCL) supplies the reactive power to the system during fault recovery. The capacitor is triggered in the system through the controller, which makes CB-SFCL performance superior to resistive SFCL [60]. Modified bridge resistive SFCL (MBR-SFCL) proposed in the literature [61] outperforms conventional SFCL. The controller duty cycle varies with system performance, which makes it superior.

A flux coupling type SFCL has been proposed and a comparative analysis has been done by placing the proposed scheme on the rotor and stator side respectively. Performance analysis shows that the proposed scheme placed on the stator side is better at maintaining the terminal voltage than placing it at the rotor side [62]. Voltage compensation type SFCL has higher controllability compared to resistive and inductive SFCL [63]. Cooperative control of SFCL, along with SMES [64] and reactive power [65], contributes to limiting the overcurrent bypassing the surplus power towards SMES during a fault.

2.6 Non-superconducting Fault Current Limiter

The other approach in this solution is N-SFCL shown in Fig 2. 3. N-SFCL usually has two parts: the bridge and the shunt impedance path. The bridge path carries power during normal operation. During a fault, the bridge part is turned off with IGBT and power flows through a high impedance path, limiting the overcurrent. In bridge type FCL (BFCL), the resistor and inductor are connected in series in the shunt path [66]. The IGBT pulse is generated with the control circuit sensing the system parameter of DFIG [67]. A capacitor replaces the inductor in BFCL to form a capacitive bridge type FCL (CB-FCL).

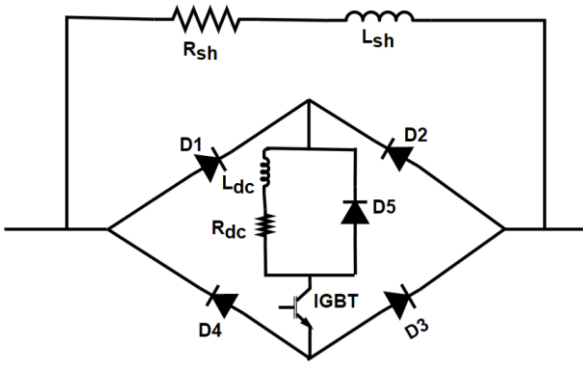

a) BFCL configuration

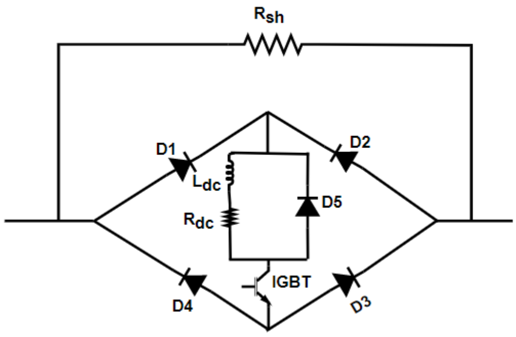

b) NC-MBFCL configuration

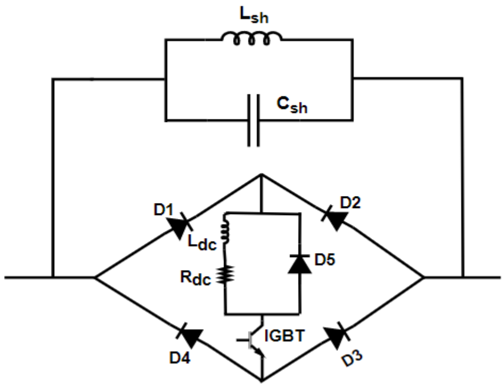

c) PRFCL configuration

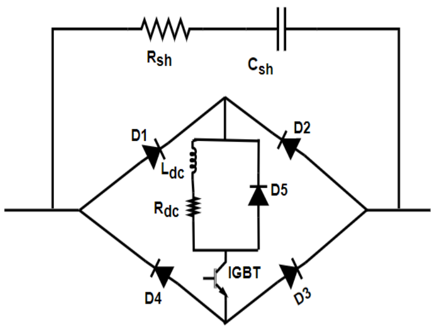

d) CB-FCL configuration

Fig 2. 3: Configuration diagrams of N-SFCL

The presence of a capacitor supports the grid voltage with the supply of reactive power [68]. Non-linear controlled modified BFCL (NC-MBFCL) consists of only one resistor in the shunt path. A non-linear control system provides the variation in shunt impedance with a change in system parameters during a fault, which makes the system superior to conventionally controlled MBFCL and BFCL [30]. The inductor and capacitor are placed in parallel in the shunt path to form the parallel resonance BFCL (PRFCL). Observation shows that PRFCL maintains mechanical torque balance in the turbine generator system, contributing to LVRT enhancement [69].

From the literature review, it is found that different strategies are being tested and implemented for DFIG's protection during a fault and to fulfill the grid code to maintain system stability. Those protection schemes are usually designed considering the worst-case scenario of maximum sag in the power system. Hence, the system response is good for the 0 dip. The system will implement the same value of impedance when the voltage drops below a reference value without analyzing the severity of the fault. But the dip in the bus voltage will not always be the same. Designing the FCL impedance for one case and implementing the same impedance for all cases will not produce good responses. In the case of a less severe fault, the whole impedance value overloads the DFIG, which will add more disturbance to the system. To overcome this problem, a ladder resistive fault current limiter (LRFCL) is proposed in this thesis. The major aim of LRFCL is to analyze the bus voltage and trigger the desired resistance level. Thus, bulk SDBR resistance can be broken down into the desired steps and a control circuit can be designed to select the appropriate resistance level with the different levels of a dip in bus voltage. Later on, fuzzy control based FCL is developed and analyzed to precisely control the power being dropped in the external resistance during the variation in bus voltage.

Chapter 3

System Model

3.1 DFIG System Overview

A schematic diagram of the DFIG connected to the power grid and the local load is shown in Fig 3. 1. The stator of the DFIG is connected directly to the grid while the rotor is connected to the back-to-back converter (RSC and GSC) through the slip ring. The role of the RSC converter is to control the rotor voltage and frequency to stabilize the stator voltage and frequency to the desired value. The HAWT drives the turbine connected to the DFIG. The objective of GSC is to maintain the DC-link voltage. Being the bidirectional converter, power can flow in both directions in RSC and GSC converters. During super synchronous operation, active power will flow towards the grid while in sub synchronous operation active power is consumed from the grid. Thus, DFIG can work both in the sub-synchronous and super synchronous modes. Stator power flow is unidirectional. Power is always transferred to the grid from the stator. The equation that relates ω_s (frequency of stator voltages and currents), ω_r (frequency of rotor voltages and currents) and ω_m (rotor electrical speed) is as follow [70]:

$$\omega_s = \omega_r + \omega_m \tag{3.1}$$

Mechanical speed of the shaft and stator voltage frequency is related as:

$$\omega_s = p\Omega_m \tag{3.2}$$

where p is the pole pair of the machine.

The units of these two equations are given in rad/s. The slip s of the machine is defined as follows:

$$s = \frac{\omega_s - \omega_m}{\omega_s} = \frac{\omega_r}{\omega_s} \tag{3.3}$$

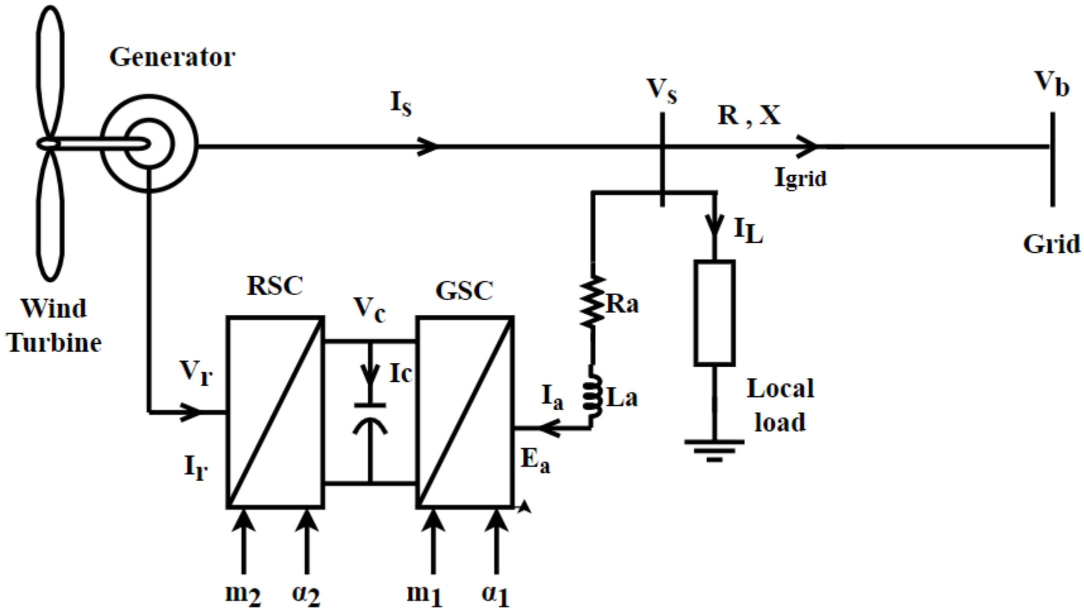

Fig 3. 1: DFIG system configuration

The stator windings are directly connected to the grid and thus, ω_s is constant. This frequency is also known as the synchronous frequency. However, ω_r depends on the shaft's electrical speed ω_m, which leads to three operating modes of the machine depending on the speed [70]:

$\omega_m < \omega_s \Rightarrow \omega_r > 0 \Rightarrow s > 0 \Rightarrow$ Sub synchronous operation

$\omega_m > \omega_s \Rightarrow \omega_r < 0 \Rightarrow s < 0 \Rightarrow$ Super-synchronous operation

$\omega_m = \omega_s \Rightarrow \omega_r = 0 \Rightarrow s = 0 \Rightarrow$ Synchronous operation

3.2 Wind Turbine Model

The role of a wind turbine is to convert the aerodynamic power obtained from air flow to the mechanical energy. The mechanical power output obtained from the turbine is expressed as the function of wind speed (V_w) which is expressed in [71] as:

$$P_m = \frac{1}{2}\rho A C_p(\lambda, \beta) V_\omega^3 \qquad (3.4)$$

where, ρ is the air density.

A is the area swept by the turbine blade.

C_p is the power coefficient.

β is the blade pitch angle.

Tip speed ratio (λ) is the ratio of the linear speed at the tip of blades to the wind speed. The expression for the λ is given as:

$$\lambda = \frac{\Omega_m R}{V_w} \qquad (3.5)$$

R is the radius of the wind turbine rotor.

Power coefficient indicates the efficiency of the wind turbine. It is the ratio of the mechanical power to the aerodynamic power. C_p is the function of the tip speed ratio and the blade pitch angle and is expressed in [72] as:

$$C_p(\lambda, \beta) = 0.5176\left(\frac{116}{\lambda_i} - 0.4\beta - 5\right)e^{\frac{-21}{\lambda_i}} + 0.0068\lambda \qquad (3.6)$$

$$\frac{1}{\lambda_i} = \frac{1}{\lambda + 0.08\beta} - \frac{0.035}{\beta^3 + 1} \qquad (3.7)$$

Two mass model is use to express the drive train model of the generator and turbine system [73]. The electromechanical dynamics of the drive train model is expressed using the differential equation as:

$$\frac{d\omega_t}{dt} = \frac{1}{2H_t}(P_m - K_s\theta_s - D_t\Delta\omega_t) \tag{3.8}$$

$$\frac{d\omega_r}{dt} = \frac{1}{2H_g}(K_s\theta_s - P_e - D_g\Delta\omega_r) \tag{3.9}$$

$$\frac{d\theta_s}{dt} = \omega_0(\omega_t - \omega_r) \tag{3.10}$$

Where D_g and D_t are the damping coefficient of the generator and turbine. K_s is the shaft stiffness and θ_s is the torsion angle.

The turbine connected through the gearbox and shaft system is use to rotate the rotor of the DFIG and electricity is generated. The electric power output of the DFIG is expressed as:

$$P_e = x_m i_{rq} i_{sd} - x_m i_{rd} i_{sq} \tag{3.11}$$

3.3 DFIG Model

The instantaneous or time varying expression of the stator voltage, current and fluxes with respect to abc reference frame of the DFIG is given as:

$$v_{as}(t) = R_s i_{as}(t) + \frac{d\psi_{as}(t)}{dt}$$

$$v_{bs}(t) = R_s i_{bs}(t) + \frac{d\psi_{bs}(t)}{dt} \quad (3.12)$$

$$v_{cs}(t) = R_s i_{cs}(t) + \frac{d\psi_{cs}(t)}{dt}$$

Similarly, stator voltage, current and fluxes with respect to abc reference frame of the DFIG is given as:

$$v_{ar}(t) = R_r i_{ar}(t) + \frac{d\psi_{ar}(t)}{dt}$$

$$v_{br}(t) = R_r i_{br}(t) + \frac{d\psi_{br}(t)}{dt} \quad (3.13)$$

$$v_{cr}(t) = R_r i_{cr}(t) + \frac{d\psi_{cr}(t)}{dt}$$

Applying the Park's transformation i.e., abc to dq transformation of the voltage, current and flux, we get the following expression [74]:

$$\vec{v}_s^a = R_s \vec{i}_s^a + \frac{d\vec{\psi}_s^a}{dt} + \mathrm{j}\omega_s \vec{\psi}_s^a \;\Rightarrow\; \begin{Bmatrix} v_{sd} = \mathrm{R}_s i_{sd} + \frac{d\psi_{sd}}{dt} - \omega_s \psi_{sq} \\ v_{sq} = \mathrm{R}_s i_{sq} + \frac{d\psi_{sq}}{dt} + \omega_s \psi_{sd} \end{Bmatrix} \quad (3.14)$$

$$\vec{v}_r^a = R_r \vec{i}_r^a + \frac{d\vec{\psi}_r^a}{dt} + \mathrm{j}\omega_r \vec{\psi}_r^a \;\Rightarrow\; \begin{Bmatrix} v_{rd} = \mathrm{R}_s i_{rd} + \frac{d\psi_{rd}}{dt} - \omega_r \psi_{rq} \\ v_{rq} = \mathrm{R}_r i_{rq} + \frac{d\psi_{rq}}{dt} + \omega_r \psi_{rd} \end{Bmatrix} \quad (3.15)$$

Transformation of the stator and rotor flux in to d-q frame is:

$$\vec{\psi}_s^a = L_s \vec{i}_s^a + L_m \vec{i}_r^a \;\Rightarrow\; \begin{Bmatrix} \psi_{sd} = L_s i_{sd} + L_m i_{rd} \\ \psi_{sq} = L_s i_{sq} + L_m i_{rq} \end{Bmatrix} \quad (3.16)$$

$$\vec{\psi}_r^a = L_m \vec{i}_s^a + L_r \vec{i}_r^a \quad \Rightarrow \begin{Bmatrix} \psi_{rd} = L_m i_{sd} + L_r i_{rd} \\ \psi_{rq} = L_m i_{sq} + L_r i_{rq} \end{Bmatrix} \tag{3.17}$$

The d-q component of the stator and the rotor current is expressed as:

$$\begin{bmatrix} \frac{di_{sd}}{dt} \\ \frac{di_{rd}}{dt} \end{bmatrix} = Z \begin{bmatrix} \omega_0 R_s & 0 & \omega_e x_s & -\omega_e x_m \\ 0 & \omega_0 R_r & -s\omega_0 x_m & -s\omega_0 x_m \end{bmatrix} [i_g] + \begin{bmatrix} \omega_0 v_{sd} \\ \omega_0 v_{rd} \end{bmatrix} \tag{3.18}$$

$$\begin{bmatrix} \frac{di_{sq}}{dt} \\ \frac{di_{rq}}{dt} \end{bmatrix} = Z \begin{bmatrix} \omega_e x_s & \omega_e x_m & \omega_0 R_s & 0 \\ s\omega_0 x_m & s\omega_0 x_r & 0 & \omega_0 R_r \end{bmatrix} [i_g] + \begin{bmatrix} \omega_0 v_{sq} \\ \omega_0 v_{rq} \end{bmatrix} \tag{3.19}$$

Where Z= $\begin{bmatrix} -x_s & -x_m \\ -x_m & -x_r \end{bmatrix}^{-1}$

Here subscript s and r is use to denote stator and rotor and d and q defines d-axis and q-axis component respectively.

3.4 Converter and Load Model

Converters and local load model are modelled as mentioned in [75][76].

The rotor voltage relating the DC-link voltage is expressed as:

$$\begin{aligned} v_{rd} &= m_2 V_c cos\alpha_2 \\ v_{rq} &= m_2 V_c sin\alpha_2 \end{aligned} \tag{3.20}$$

Power in the rotor side is given by:

$$P_r = v_{rd} i_{rd} + v_{rq} i_{rq} \tag{3.21}$$

The output voltage on the filter side of the GSC converter is linked with DC-link voltage as:

$$\begin{aligned} e_{ad} &= m_1 V_c cos\alpha_1 \\ e_{aq} &= m_1 V_c sin\alpha_1 \end{aligned} \tag{3.22}$$

Power on the output of the GSC converter i.e., power towards the filter side is expressed as:

$$P_f = e_{ad}i_{ad} + e_{aq}i_{aq} \tag{3.23}$$

Here, m_1, α_1 and m_2, α_2 are the modulation index and the phase angle of the GSC and RSC respectively. Here subscript 'a' is use to denote filter.

The d-q component of the GSC current or the current flowing through the filter is expressed using the differential equation as:

$$\begin{bmatrix} \frac{di_{ad}}{dt} \\ \frac{di_{aq}}{dt} \end{bmatrix} = \frac{\omega_0}{L_a}\begin{bmatrix} -R_a & (1-\Delta\omega_e)L_a \\ -(1-\Delta\omega_e)L_a & -R_a \end{bmatrix}\begin{bmatrix} i_{ad} \\ i_{aq} \end{bmatrix} + \frac{\omega_0}{L_a}\begin{bmatrix} v_{sd} - e_{ad} \\ v_{sq} - e_{aq} \end{bmatrix} \tag{3.24}$$

The change in the DC-link voltage results in the power imbalance between the power input to the converter and the power flowing out from the converter. If the converters are supposed to be lossless than during the steady state condition power in and out must be equal so the expression for the DC-link voltage is given as:

$$P_{DC} = CV_c\frac{dV_c}{dt} \tag{3.25}$$

Also,

$$P_{DC} = P_f - P_r \tag{3.26}$$

$$\frac{dV_c}{dt} = \frac{1}{CV_c}\left(e_{ad}i_{ad} + e_{aq}i_{aq} - v_{rd}i_{rd} - v_{rq}i_{rq}\right) \tag{3.27}$$

$$\frac{dV_c}{dt} = \frac{1}{C}\left(m_1cos\alpha_1i_{ad} + m_1sin\alpha_1i_{aq} - m_2cos\alpha_2i_{rd} - m_2sin\alpha_2i_{rq}\right) \tag{3.28}$$

Local load is connected to the terminal of the stator. The admittance of the local load is given as:

$$Y_{11} = g_{11} + b_{11} \tag{3.29}$$

Current flowing through the local load is:

$$I_L = V_s Y_{11} \tag{3.30}$$

Impedance of the transmission line connecting the DFIG stator to the bus is model as:

$$Z_{12} = R + jX \tag{3.31}$$

Hence current flowing through the transmission network is:

$$I_{grid} = \frac{V_s - V_b}{R + jX} \tag{3.32}$$

Applying KCL at the terminal of the stator,

$$I_s - I_a = I_{grid} + I_l \tag{3.33}$$

$$I_{grid} + I_l = (i_{sd} - i_{ad}) + j(i_{sq} - i_{aq}) \tag{3.34}$$

Since fault current is the resistive element and it is connected in series in the grid side during the faulty condition so the expression for the grid current during the application of FCL is given as:

$$I_{grid} = \frac{V_s - V_b}{(R + R_{ext}) + jX} \tag{3.35}$$

Where R_{ext} is the value of the resistance of the FCL and its value depends on the type of system being used as the FCL which is described in detail in chapter 4.

3.5 The Composite Dynamic Model

A composite state space model of the DFIG system shown in Fig 3. 1 is obtained by equating the KCL at the stator terminal.

Stator current – Converter current = Grid current + Load current

$$I_s - I_a = I_{grid} + I_L \tag{3.36}$$

$$I_S - I_a = (V_S - V_b)Y_{12} + V_S Y_{11} \tag{3.37}$$

$$V_s = \frac{1}{Y_{11} + Y_{12}}(I_s - I_a + V_b Y_{12}) \tag{3.38}$$

During normal operating condition

$$Y_{12} = \frac{1}{R + jX} \tag{3.39}$$

During activation of FCL

$$Y_{12} = \frac{1}{(R + Rext) + jX} \tag{3.40}$$

d and q axes component of stator voltage is calculated as:

$$\begin{aligned} V_{sd} &= real(V_s) \\ V_{sq} &= imag(V_s) \end{aligned} \tag{3.41}$$

Substituting V_{sd} and V_{sq} in equation 3.18 and 3.19, the derivative of the stator and rotor current i_{sd} , i_{sq} , i_{rd} and i_{rq} is obtained. Two mass model gives the differential equation for angular speed of generator rotor, angular speed of turbine and shaft torsion angle as shown in equation 3.8, 3.9 and 3.10 respectively. Equation 3.24 gives the differential equation for grid converter side current. Differential equation for converter DC-link voltage is given in equation 3.28. Those equations are combined to give closed form state equations,

$$\dot{X} \quad = f[X, u] \tag{3.42}$$

Where the state vector X is given as

$X = [i_{sd}, i_{sq}, i_{rd}, i_{rq}, \omega_t, \omega_r, \theta_s, V_c, i_{ad}, i_{aq}]$

u is the vector of converter controls $[m_1, m_2, \alpha_1, \alpha_2]$

Chapter 4

Fault Current Limiter Modeling and Control

4.1 Series Dynamic Braking Resistor Modeling and Control

The basic model of SDBR is shown in Fig 4. 1. It consists of two parts, a resistor and the power electronics IGBT switch. The switching operation of an IGBT is controlled by the voltage signal provided to the gate. A high signal (1) at the gate will turn it on, while a low signal (0) will turn it off. Electronic switches are quick in operation as there is no mechanical movement during operation. The SDBR circuit has two paths for the current to flow. During normal operation, the IGBT switch will remain closed and the current will flow through the low resistance path. Since R_{SDBR} is high, negligible current will flow through it. Hence, the loss is minimum.

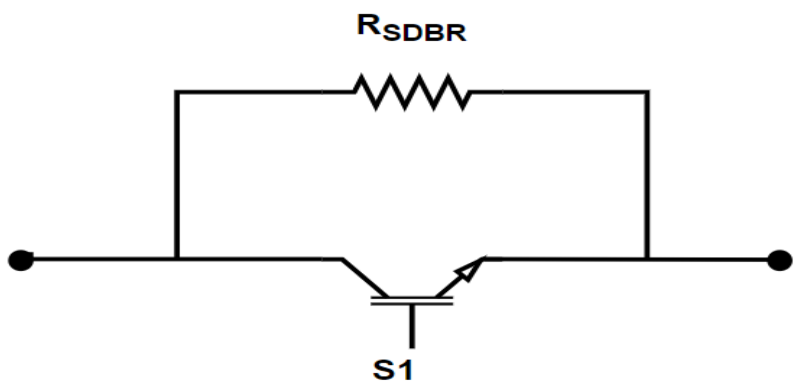

Fig 4. 1: Configuration of SDBR

During the fault, the switch will be open and the current will flow through a high resistance path. The high value of the series resistor will limit the overcurrent. The series resistor will consume the generator's active power. The circuit diagram for the generation of the IGBT gate pulses is shown in Fig 4. 2. When the bus voltage falls below the reference voltage (0.9 pu in this case), the comparator output will be high. The output signal is inverted and passes through the IGBT pulse generator, which will open the IGBT switch. Current will be forced through the high resistance path. The resistor will remain connected to the system until the normal voltage level is reached after the clearance of the fault in the system. Once the system voltage is recovered, the IGBT switches will be closed and normal operating conditions will be restored.

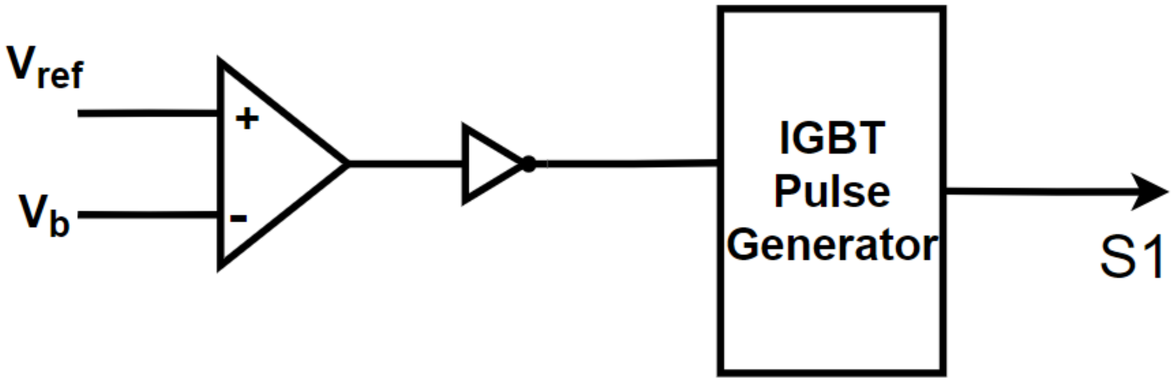

Fig 4. 2: SDBR switching signal generation circuit

The value of resistance of SDBR to drop the surplus power during the 0-voltage dip in the bus terminal is calculated as [77][78]:

Active power output from stator = 0.8998 pu

Active power output from rotor = 0.04 pu

Total active output power from DFIG (P)= $Ps + Pr$

Admittance of local load (Y)= $g11 + j * b11$

$=0.403 + j0.1014$

Impedance of local load(Z) = $r11 + j * x11 = \frac{1}{Y}$ $=2.2336 - j * 0.5871$

Active power consumed by local load (P_L)= $\frac{(V_t)^2}{r11} = \frac{1.0299^2}{2.3336} = 0.4545\ pu$

Power transferred to line P_{line}= $P - P_L$=$0.4853\ pu$

Series resistance required to consume active power in line =$\frac{(V_t)^2}{P_{line}} - R = 2.1356\ pu$

Hence the required resistance value of SDBR is 2.1356 pu.

4.2 Resistive Superconducting Fault Current Limiter Modeling

The superconducting fault current limiter (SFCL) is one of the reliable solutions for enhancing the LVRT of the DFIG. With a sudden rise in the current passing through the superconductor, the behavior of the superconductor changes from the superconducting state to a resistive state. This phenomenon is known as quenching. Furthermore, once the fault is cleared, the current will decrease and the superconductor will gradually regain its superconducting state, a process known as recovery. The operating characteristics of RSFCL with quenching and recovery phenomena are shown in Fig 4. 3.

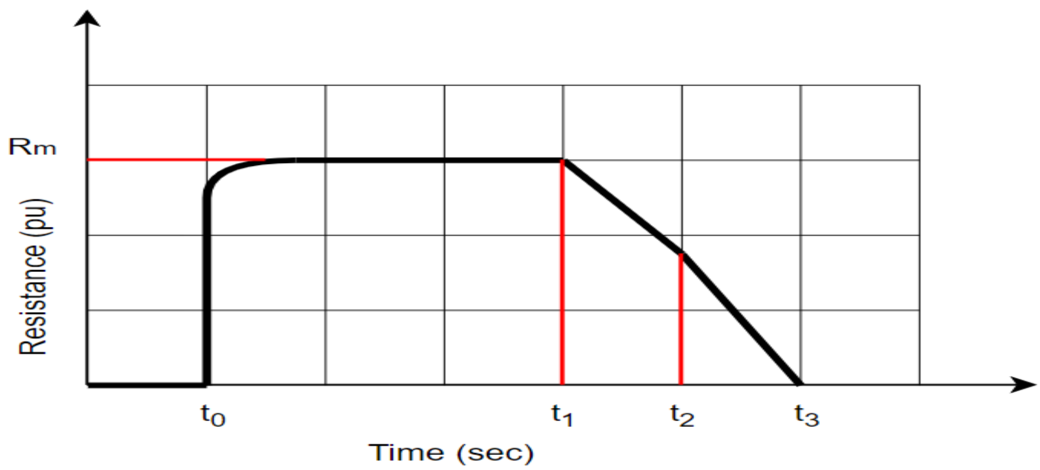

Fig 4. 3: Quenching and recovery characteristics of RSFCL

The mathematical model of the resistive SFCL is given as [79][80]:

$$R_{SFCL} = \begin{cases} 0 & t > t_0 \\ R_m[1 - \exp\left(-\frac{t-t_0}{T_f}\right)]^{1/2} & t_0 \leq t < t_1 \\ a_1(t-t_1)+b_1 & t_1 \leq t < t_2 \\ a_2(t-t_2)+b_2 & t_2 \leq t < t_3 \end{cases} \quad (4.1)$$

Where, Rm is the maximum resistance of the SFCL in the quenching state, T_f is the time constant of the SFCL during transition from superconducting state to normal state, t_0 is the time to start the quenching, t_1 is the 1st recovery time, t_2 is the 2nd recovery time, t_3 is the complete recovery time. a_1, a_2, b_1 and b_2 are the constants whose values are given in Appendix B. For comparison, R_m is kept the same as that of R_{SDBR}.

The advantage of R-SFCL over SDBR is that due to the self-quenching nature of R-SFCL, there is no requirement for the external control system and switches for its activation during fault. R-SFCL will be always in series in the protection circuit. Resistance will increase automatically upon reaching the current or thermal threshold. The developed system will work without the need of any sensors. There is no chance for the system to fail due to failure in the control system or the sensor devices. But the problem is that R-SFCL is costly to implement as superconductors are expensive. For any level of voltage sag, the whole resistive value will be applied to the system.

4.3 Ladder Resistive Fault Current Limiter Modeling and Control

The magnitude or level of voltage sag in the power system is not constant. Voltage sag magnitude is affected by a various factor, including the distance between the observation and the fault source, the type of fault, fault impedance, and the voltage in the system prior to the occurrence of the fault. Different natures of faults can cause varying levels of voltage dip in the system. Usually, the fault current limiter is designed considering the worst-case scenario of the maximum sag in the system voltage. It will not produce a good result when the same impedance value is triggered in the system without considering the voltage sag level. For less severe faults, the voltage dip level is less. Inserting the whole impedance value designed for the maximum sag to the low sag condition will not support the system's transient stability due to the generator's overloading.

The problem with conventional FCL (SDBR) and RSFCL is that they will insert the same impedance value into the system through the series compensating device without considering the level of voltage sag and severity of the fault. In order to address this issue, a new control strategy has been proposed which considers the level of dip in the bus voltage. For this, the ladder network is designed to break the whole resistance value into two parts. Hence, LRFCL is designed considering two ladder levels of resistance.

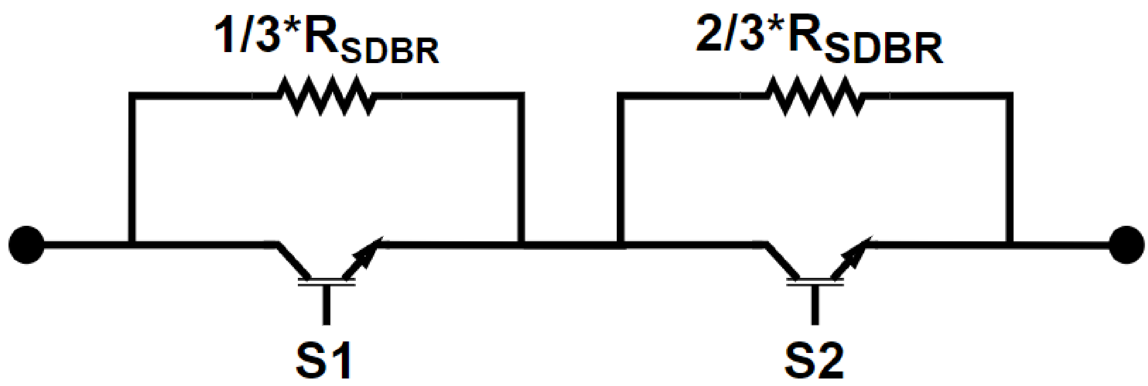

Fig 4. 4: Configuration of LRFCL

The configuration of LRFCL is shown in Fig 4. 4. Here the resistance value calculated in the SDBR is divided into two parts i.e., R/3 and 2*R/3. The two sections of the LRFCL are controlled through the semiconductor switches S1 and S2. The algorithm used for the generation of the IGBT switches pulses is shown in the flowchart in Fig 4. 5.

Impedance offered by LRFCL for different levels of voltage dip is given by equation:

$$R_{LRFCL} = \begin{cases} 0 & V_b > 0.9 \\ \frac{1}{3} * R_{SDBR} & 0.6 < V_b \leq 0.9 \\ \frac{2}{3} * R_{SDBR} & 0.4 < V_b \leq 0.6 \\ R_{SDBR} & V_b \leq 0.4 \end{cases} \tag{4.2}$$

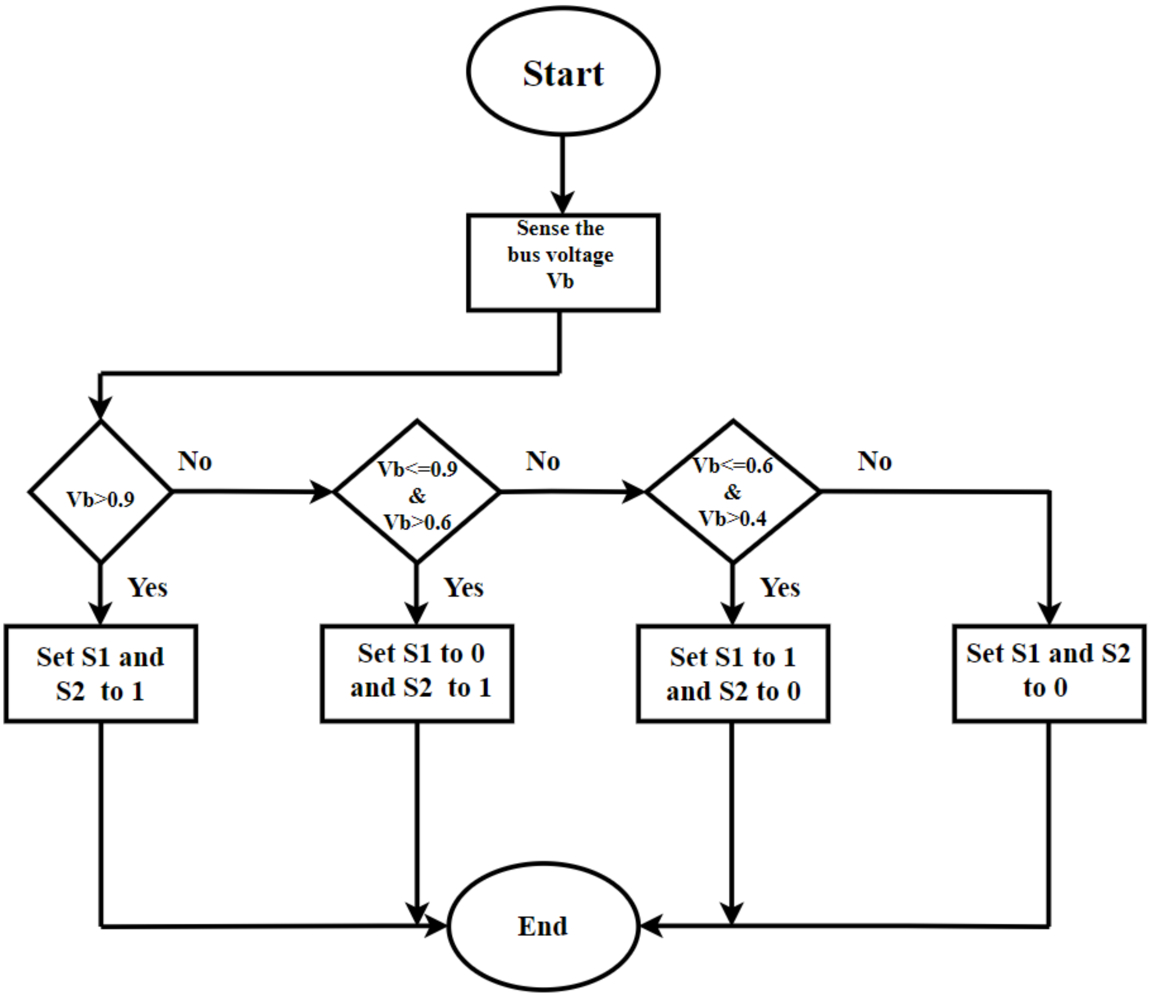

Fig 4. 5: Flow chart for generation of control signal of IGBT switches.

With the control algorithm, three different levels of resistance can be triggered in the system depending on the bus voltage. When bus voltage falls below 0.4 pu both S1 and S2 will be set low (0). LRFCL offers full resistance to the system. For bus voltage between 0.4 pu and 0.6 pu, S1 will be high (1) and S2 will be low (0), so a 2*R/3 value of resistance will be activated in the system. When the bus voltage is between 0.6 pu and 0.9 pu, S1 will be low and S2 will be high. R/3 value of resistance will be triggered in series. The threshold reference voltage is set to 0.9 pu in this case. This means if the bus voltage falls below the reference value, the system will interpret it as a fault. Above 0.9 pu bus voltage, S1 and S2 will be set high, providing the lowest resistance path for the DFIG power flow. The circuit diagram for the generation of the switching signal of the IGBT switches is shown in Fig 4. 6.

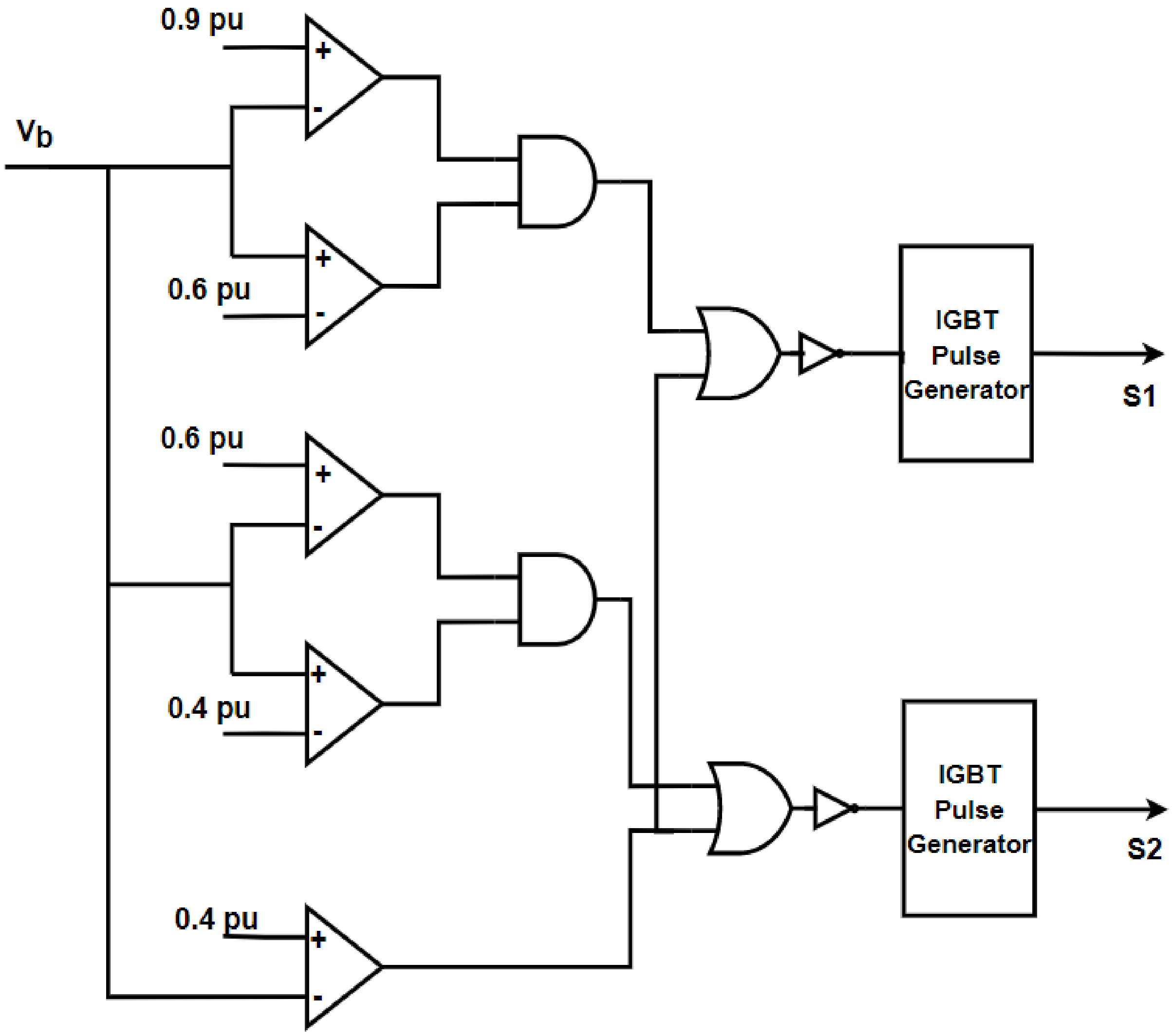

Fig 4. 6: Control circuit for generation of IGBT pulses for LRFCL

4.4 Fuzzy Logic Control Based SDBR

A fuzzy logic-based control system is designed to control the SDBR for various levels of voltage dip. A fuzzy logic controller (FLC) is used to generate the duty cycle (d). The functional block of the fuzzy inference system (FIS) showing the flow of the working mechanism of the fuzzy-based control system is given in Fig 4. 7.

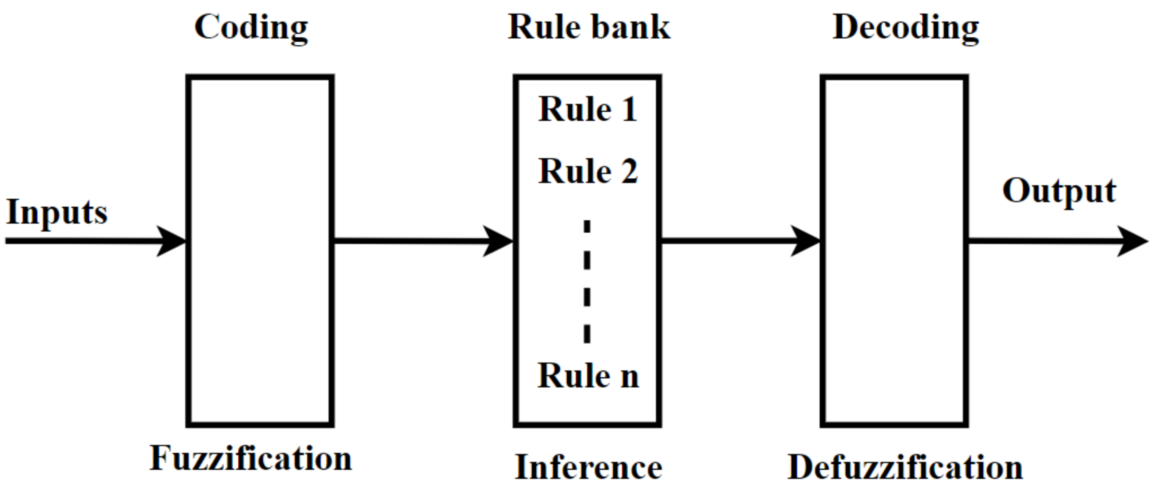

Fig 4. 7: Functional block of fuzzy inference system

The bus terminal voltage (v_b) is compared with a reference voltage (V_{ref}) and the difference in magnitude between the voltages (ΔV) is calculated. The calculated voltage change is used as the input of FLC. The output of the FLC is the duty cycle (d). The duty cycle is then used to control the switching phenomenon of the IGBT. A certain threshold voltage (V_{th}) is used to detect the fault in the system. The comparator compares the bus voltage and the threshold voltage. If bus voltage is greater than the threshold voltage, the comparator output will be high. During high output from comparator selector select switch 'b', which sends a high signal to the IGBT. At the time of the fault, bus voltage is less than the threshold hence comparator output is low. During the low output of the comparator, the selector select switch 'a', which is the inverted output of the PWM generator. The PWM output is based on the duty cycle. With the varied value of the duty cycle, instead of applying the whole resistance of SDBR, the effective variable resistance is inserted into the system during a fault. In the case of maximum sag in the system, voltage deviation and the duty cycle will be high. To activate the full resistance value in the system for maximum sag duty cycle is kept as 1 once the duty cycle is above 0.8. The mathematical expression for the effective resistance is [29]:

$$R^{*} = d * R \tag{4.3}$$

The duty cycle (d) generated by the FLC is the ratio of the time for which the IGBT switch is off (T_{off}) or does not conduct to the total time period of the PWM (T_c). The control circuit for the generation of the duty cycle for controlling the IGBT switch with the implementation of the fuzzy logic is shown in Fig 4. 8 [32].

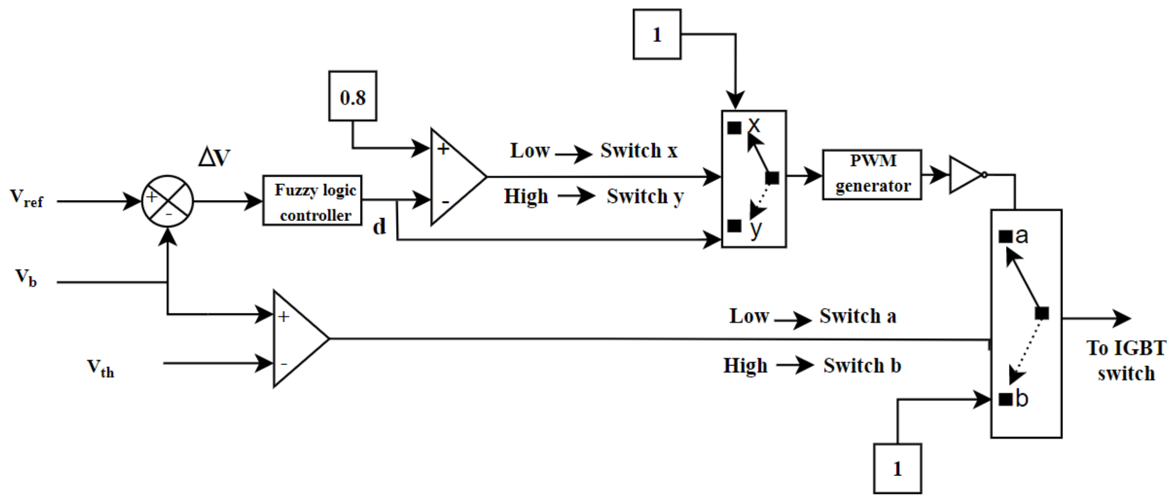

Fig 4. 8: Fuzzy logic control circuit

The mathematical expression for duty cycle is

$$d = \frac{T_{off}}{T_c} \tag{4.4}$$

$$T_c = T_{off} + T_{on} \tag{4.5}$$

T_{on} is the conduction time of the IGBT switch.

T_c is the total time period of the PWM output.

With the implementation of the FLC, the variable resistance is generated, which provides the opportunity for the system to respond dynamically to the different levels of sag in the bus voltage. The flow chart used for fuzzy based control scheme are shown in Fig 4. 9.

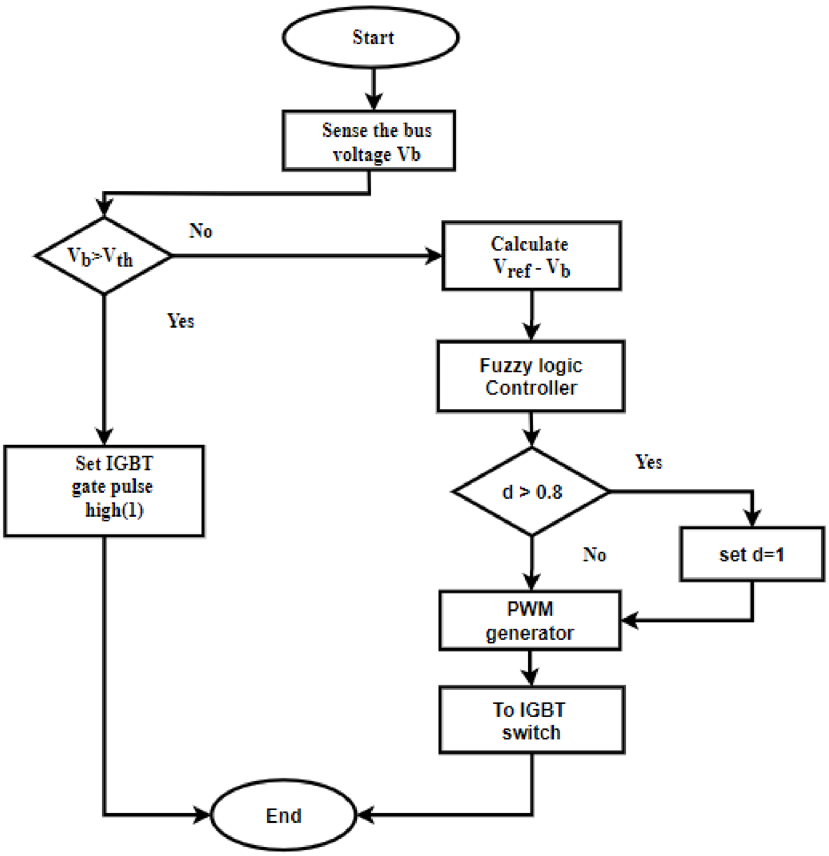

Fig 4. 9: Flow chart for generation of fuzzy based control signal

4.4.1 Membership Function in FLC

A Fuzzy membership function (MF) is an indicator that graphically represents the fuzzy sets. The membership value varies between 0 and 1. For designing the membership function, the triangular and trapezoidal membership function is used. The membership function for input (ΔV) and output (d) is shown in Fig 4. 10 and Fig 4. 11 respectively.

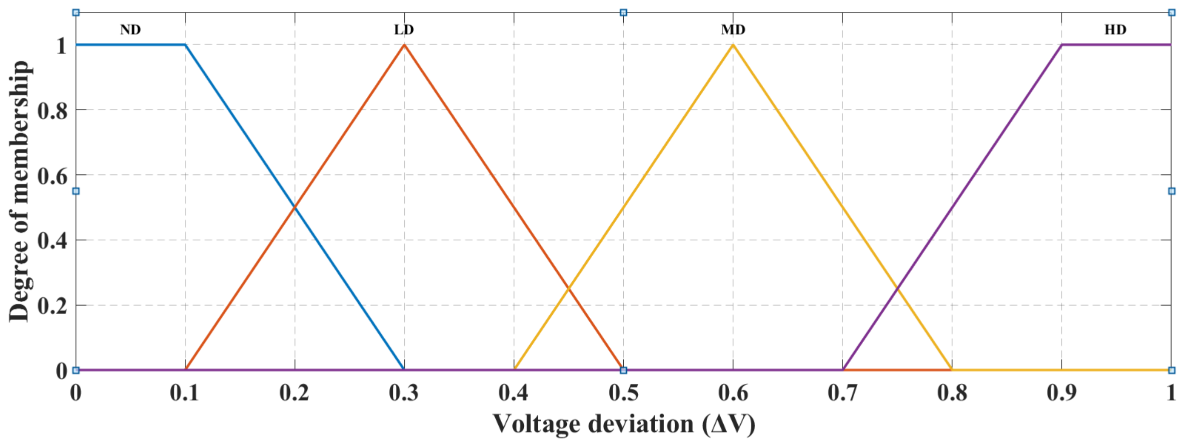

Fig 4. 10: Input membership function of fuzzy logic controller

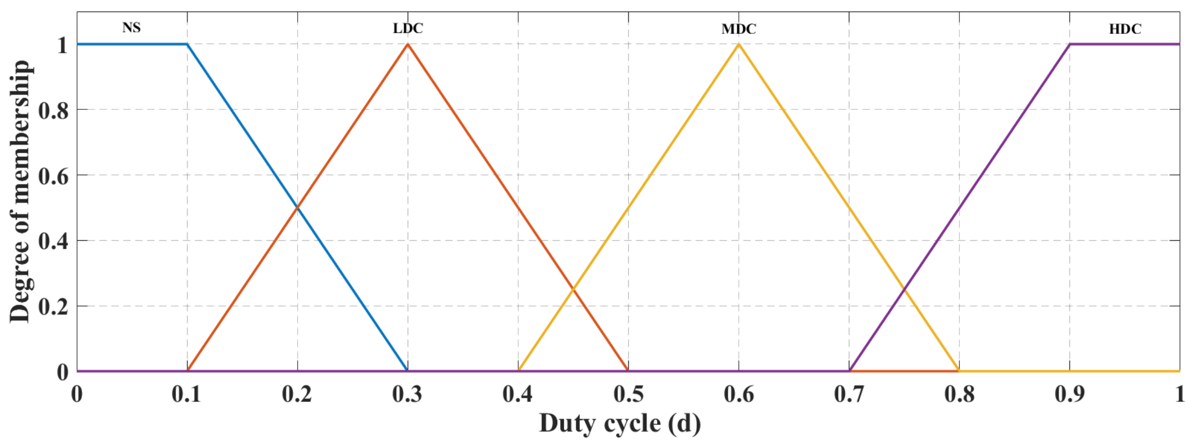

Fig 4. 11: Output membership function of fuzzy logic controller

The linguistic variables and their interpretation are given in Table 1 as:

Table 1: Interpretation of linguistic variable

ND	No deviation
LD	Low deviation
MD	Medium deviation
HD	High deviation
NS	No switching
LDC	Low duty cycle
MDC	Medium duty cycle
HDC	High duty cycle

4.4.2 Fuzzy Operation Rules

Fuzzy rules are used to get the desired output based on the inputs. In this case, it is a single input and single output-based system, so the implemented logic is simple. As the severity of the fault increases, the value of effective resistance in the system must be increased. For higher effective resistance, a higher duty cycle is required. Based on the above realization, rules for the fuzzy algorithm are developed, which are stated in Table 2.

Table 2: Fuzzy rule base

Bus Voltage Deviation (ΔV)	Duty Cycle (d)
ND	NS
LD	LDC
MD	MDC
HD	HDC

4.4.3 Fuzzy Inference Rules

A fuzzy inference system is an essential part of a fuzzy operation that facilitates decision making based on certain rules. "If and then" rules are used for the decision-making process. The output of the inference system is a fuzzy set. Later on, the defuzzification process is used to change the fuzzy variable into a crisp value. There are two types of fuzzy inference systems [81]:

ii) Mamdani fuzzy inference system

iii) Takagi Sugeno fuzzy inference system

In this research Mamdani fuzzy inference system is use because of its higher accuracy.

4.4.4 Defuzzification

Defuzzification is the process of obtaining crisp values from the fuzzy sets. There are various methods of defuzzification such as [82]:

- Center of gravity or centroid method
- Weighted average method
- Mean of maximum method

Duty cycle is calculated as the output of defuzzification through the use of center of gravity or centroid method. The defuzzification process involves the following mathematical expression:

$$d = \frac{\int \mu_A(x)\, x\, dx}{\int \mu_A(x)\, dx} \tag{4.6}$$

where $\mu_A(x)$ is the membership value for point x.

Chapter 5

Simulation Results

5.1 Simulation Consideration

The MATLAB software is used as a tool to perform the simulation. The single-line diagram of the DFIG system connected to the power system grid is shown in Fig 5. 1. DFIG is connected to the infinite bus through the transmission line. The FCL is placed in series between the terminal of the DFIG and the grid bus bar. FCL is activated through a switching mechanism during the fault. At normal operating conditions, it is in passive mode.

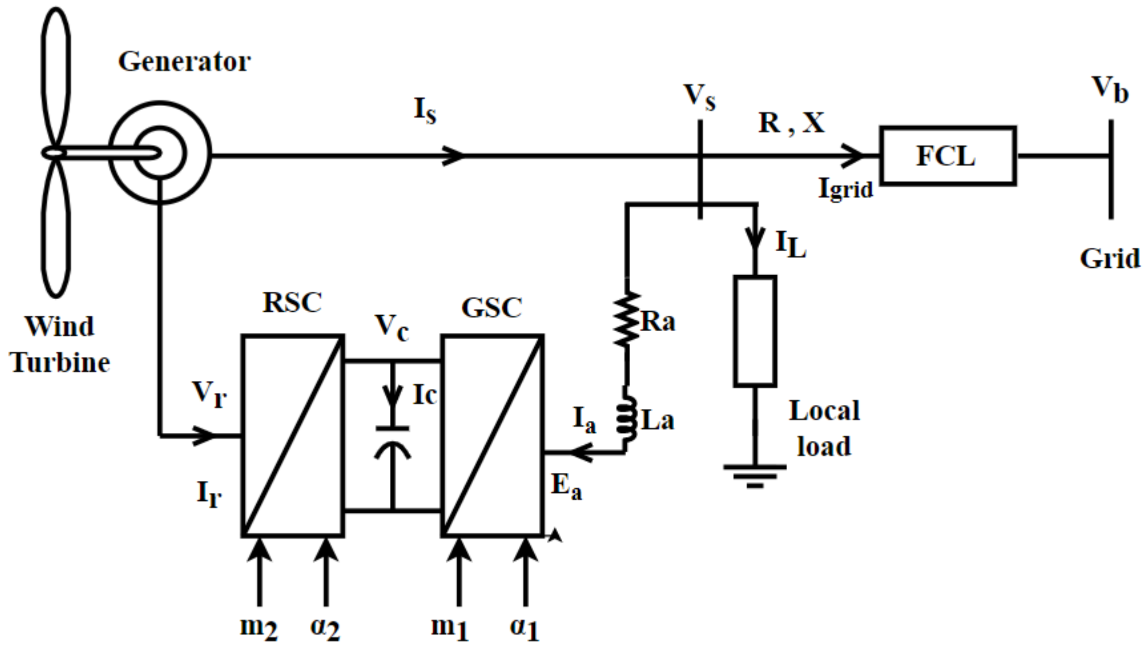

Fig 5. 1: DFIG configuration along with FCL in grid side

The mathematical model of the DFIG, its converter model and FCL is simulated in the MATLAB program. Ode45 is used to solve the non-linear equations. Wind speed is taken as 12 m/s during the study period. Since the study period is short, wind speed is considered constant. The simulation is run for 5 seconds. A fault is introduced to the system during the start of the simulation and is considered to last for 250ms.

The various series compensating devices like SDBR, R-SFCL, LRFCL and FLC-SDBR are connected in series one after another in the simulation study. During the simulation, terminal voltage, stator and rotor current, DC-link voltage, active power and generator speed are recorded. Four different control strategies are simulated one after another and the responses are recorded.

Control strategy 1: Fault analysis with SDBR

Control strategy 2: Fault analysis with R-SFCL

Control strategy 3: Fault analysis with LRFCL

Control strategy 4: Fault analysis with FLC-SDBR

5.2 Transient Stability Analysis

Three different voltage levels are considered in the bus voltage and simulation is done one after another. The different levels of bus voltage are:

Condition 1: 0 pu bus voltage

Condition 2: 0.5 pu bus voltage

Condition 3: 0.75 pu bus voltage

5.2.1 Transient Stability Analysis for 0 pu Bus Voltage

Full resistance is needed to be inserted in series in the system during the 0 pu dip in the bus voltage. Activation of LRFCL (Control strategy 3) inserts the full resistance keeping both switches S1 and S2 off. Also, during the application of FLC-SDBR (Control strategy 4) the duty cycle will be 1 for 0 dip in bus voltage activating the whole resistance value in the system as in SDBR during the fault period. Control strategy 3 and 4 are represented by control strategy 1 so only 3 control strategies are shown in this analysis. For the other 2 different cases of 0.5 pu and 0.75 pu bus voltage, all conditions are shown.

The stator and rotor currents of DFIG during the 0 pu voltage dip in bus terminal for 250 ms is shown in Fig 5. 2 and Fig 5. 3. Here we can observe that without the application of any protective scheme, stator and rotor fault current keeps oscillating and rises to 2.5 pu within 5sec. With the application of FCL, the stator and rotor currents are close to the steady state value of 0.87 pu and 0.93 pu, respectively and return to a steady state after the removal of the fault. Here we can see that RSFCL performance is better than the SDBR.

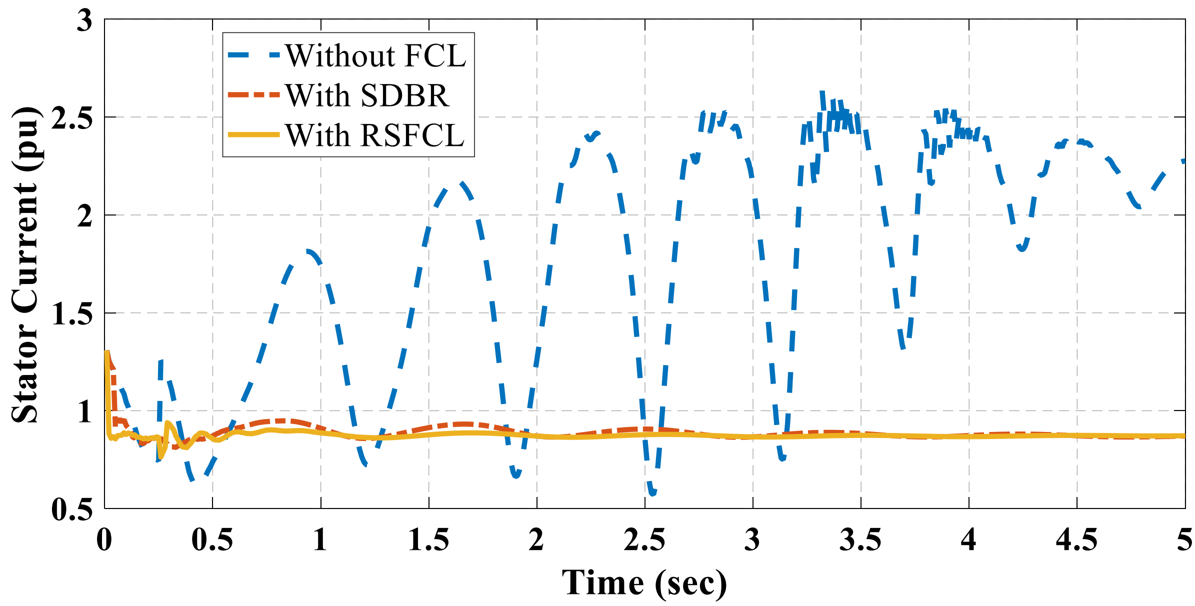

Fig 5. 2: Stator current for 0 pu dip in bus voltage

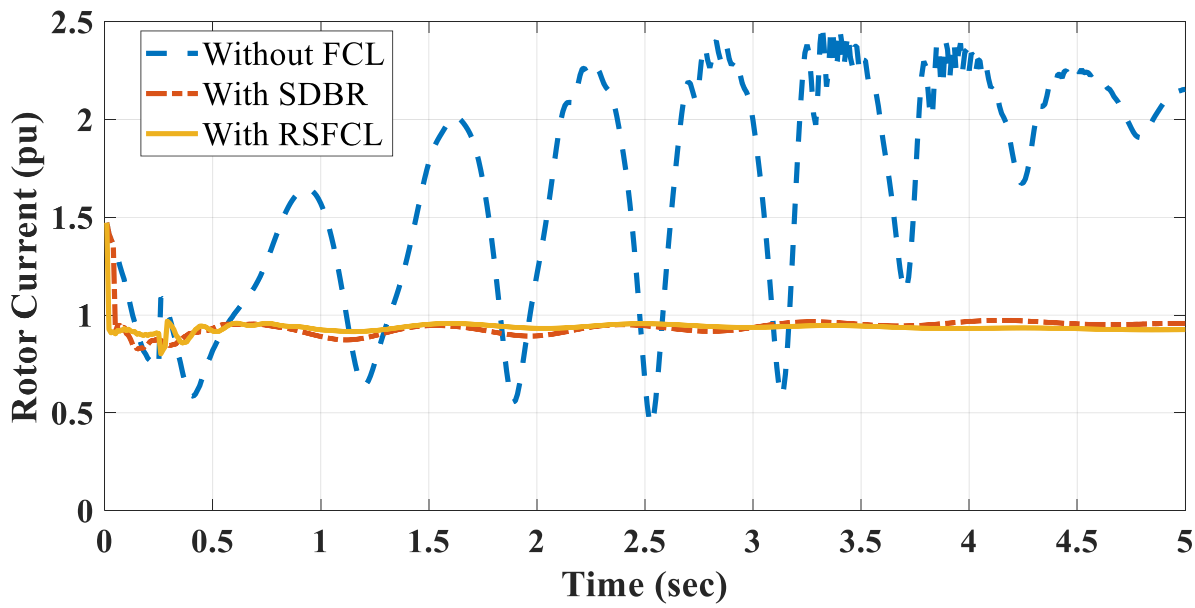

Fig 5. 3: Rotor current for 0 pu dip in bus voltage

Fig 5. 4 , Fig 5. 5 and Fig 5. 6 represent the DC-link voltage, terminal voltage and output power of the DFIG. Here it is observed that without FCL, terminal voltage and DC-link voltage do not return to the steady state after the removal of the fault. With the application of the SDBR and RSFCL, the DC-link voltage and terminal voltage are close to the steady state value of 1 pu and 1.02 pu respectively. The output power of DFIG falls to 0.5 pu without the protection scheme. With the application of FCL, it is maintained at about 0.8 pu which is close to the steady state value of 0.9 pu.

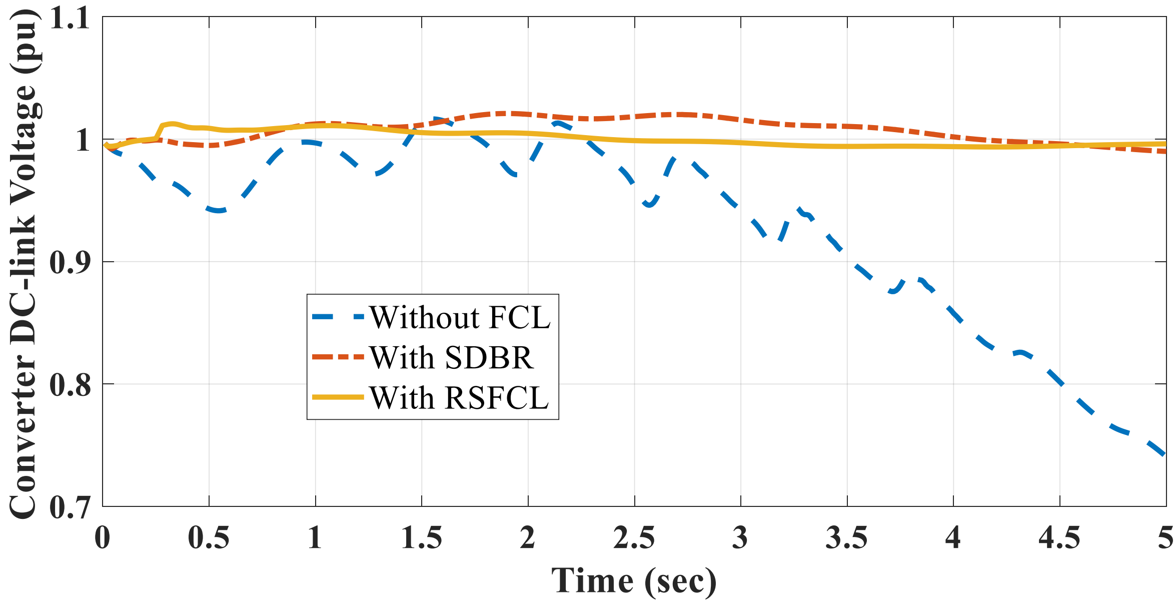

Fig 5. 4: Converter DC-link voltage for 0 pu dip in bus voltage

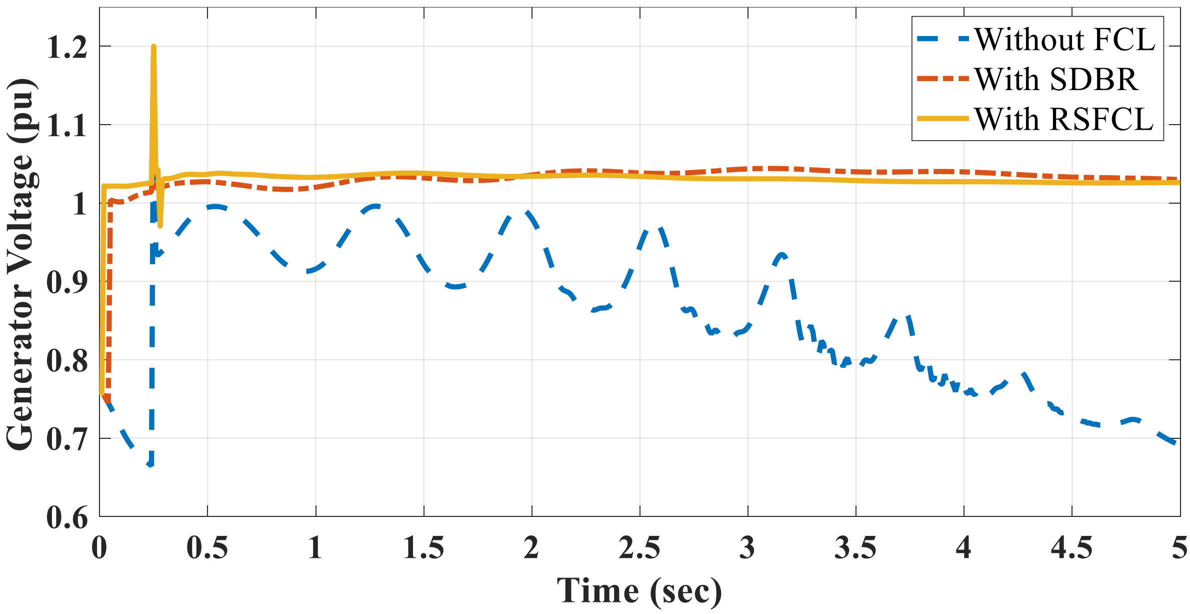

Fig 5. 5: DFIG terminal voltage for 0 pu dip in bus voltage

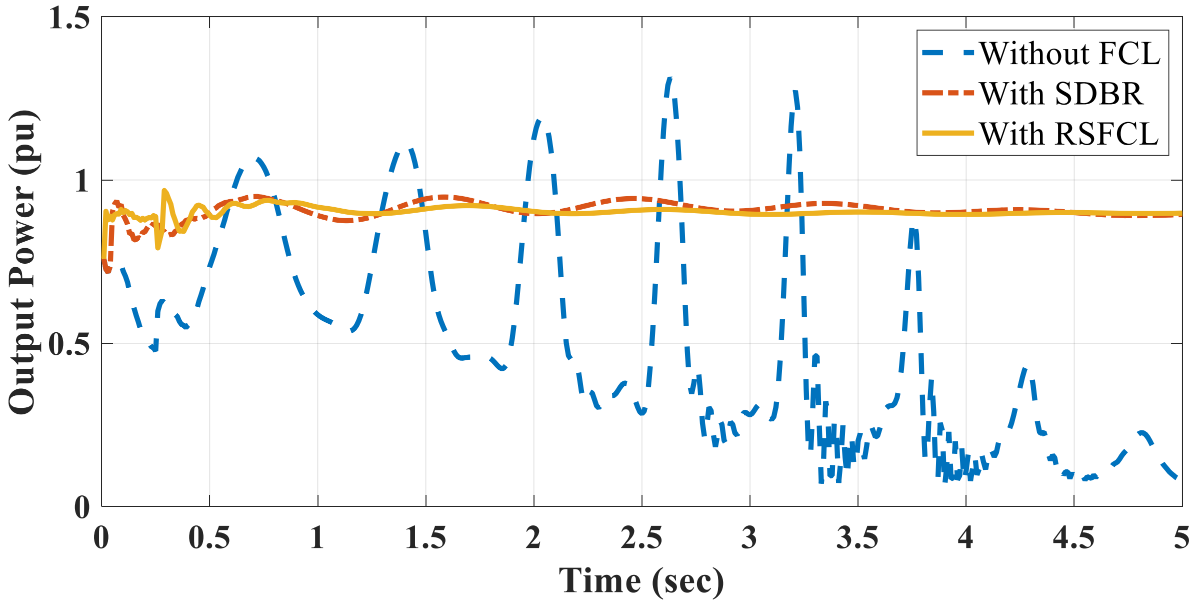

Fig 5. 6: DFIG output power for 0 pu dip in bus voltage

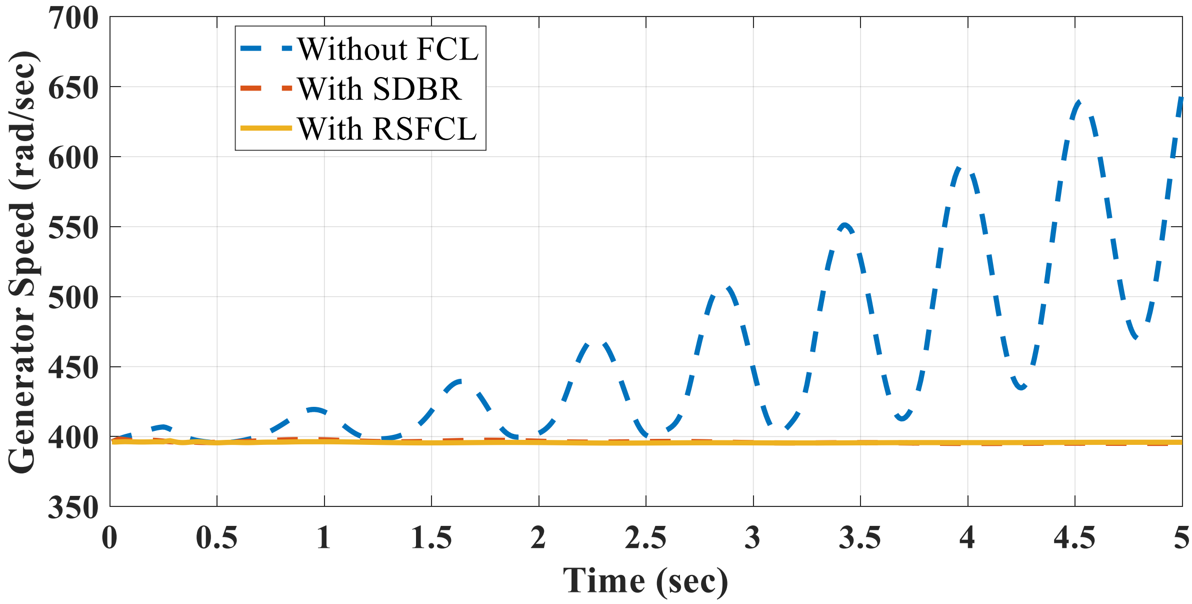

Fig 5. 7: DFIG rotor speed for 0 pu dip in bus voltage

Without the application of the FCL, the generator accelerates and rotor speed rises above 600 rad/sec within 5 seconds after the fault clearance. With the application of SDBR and RSFCL, excess power is absorbed, balancing the mechanical and electrical torque of the generator. Rotor speed is in the safe range of around 396 rad/sec which is close to the steady state value.

It is observed that without the application of a fault current limiter, voltage, current, power and speed of the DFIG keep on oscillating. The system does not return back to a steady state even after the clearance of fault in the system. After the application of the SDBR and RSFCL, voltage, current and speed of the DFIG system are in the safe operating range (close to steady state value) and the system stability is maintained.

5.2.2 Transient Stability Analysis for 0.5 pu Bus Voltage

To highlight the effectiveness of the LRFCL and FLC-SDBR over the conventional protection schemes like SDBR and RSFCL, 0.5 pu bus voltage is applied for a period of 250 ms.

Fig 5. 8 and Fig 5. 9 represent the stator and rotor current of DFIG for a voltage sag of 0.5 pu in bus voltage. Without the FCL, both the stator and rotor currents oscillate and keep rising. With the application of the LRFCL and FLC-SDBR, stator current response rises up to 0.92 pu, which is better than in the case of SDBR and RSFCL, where current rises to 0.94 pu. Observing the rotor current, we can see that with the application of SDBR and RSFCL rotor current rises up to 1.03 pu and 1.08 pu respectively. With the LRFCL and FLC-SDBR, the rotor current rises up to 0.98 pu and 0.96 pu respectively.

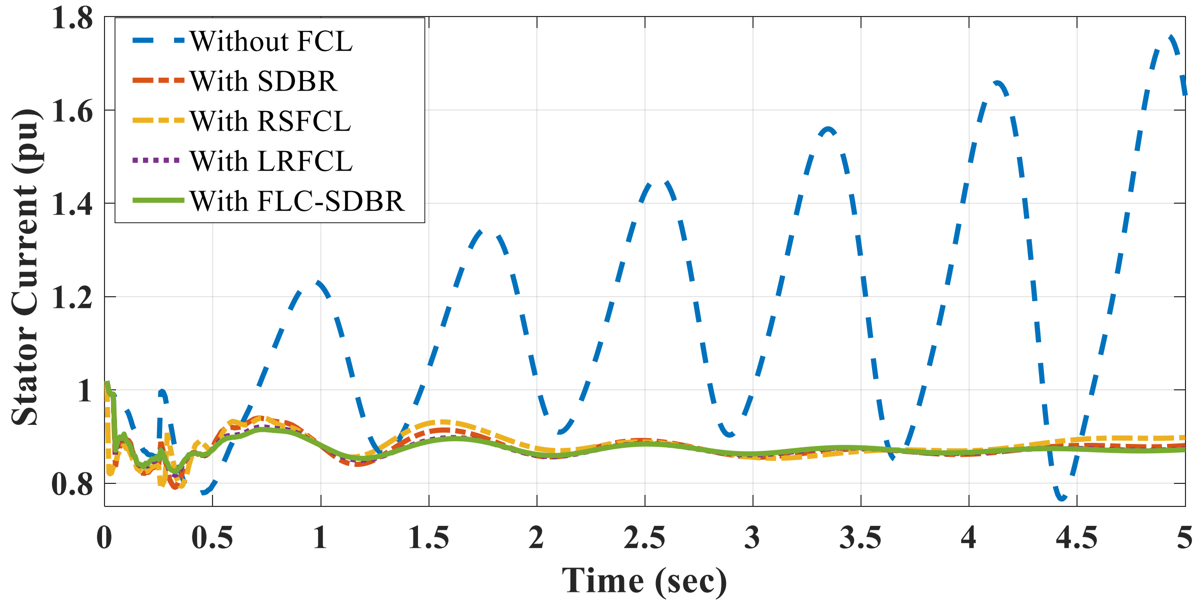

Fig 5. 8: Stator current for 0.5 pu dip in bus voltage

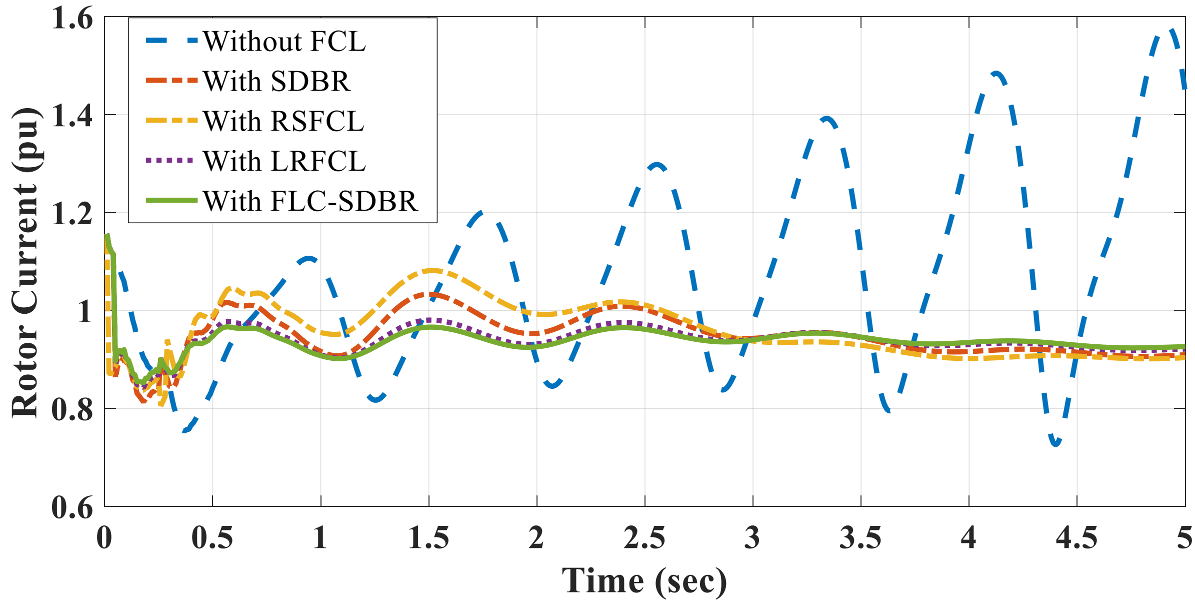

Fig 5. 9: Rotor current for 0.5 pu dip in bus voltage

Fig 5. 10 and Fig 5. 11 represent the converter DC-link voltage and the DFIG terminal voltage respectively. Here, DC-link voltage keeps rising and the terminal voltage keeps on oscillating in the absence of FCL. With RSFCL and SDBR, DC-link voltage rises to around 1.05 pu. With FLC-SDBR it is limited to about 1.01 pu. Also, oscillation is less in terminal voltage for LRFCL and FLC-SDBR compared to SDBR and R-SFCL.

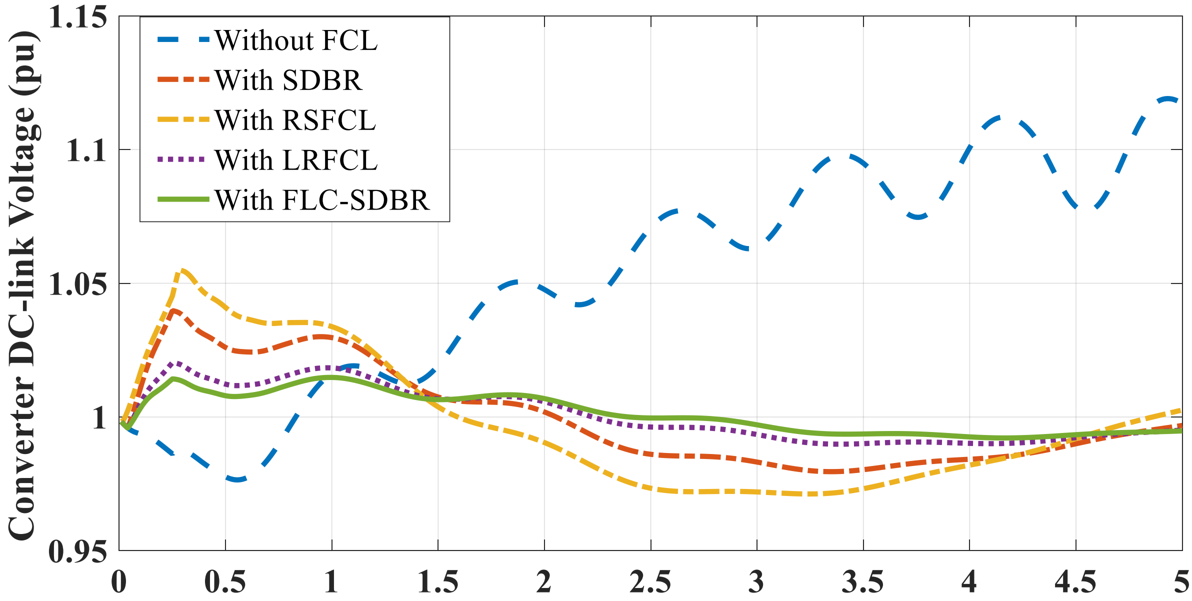

Fig 5. 10: Converter DC-link voltage for 0.5 pu dip in bus voltage

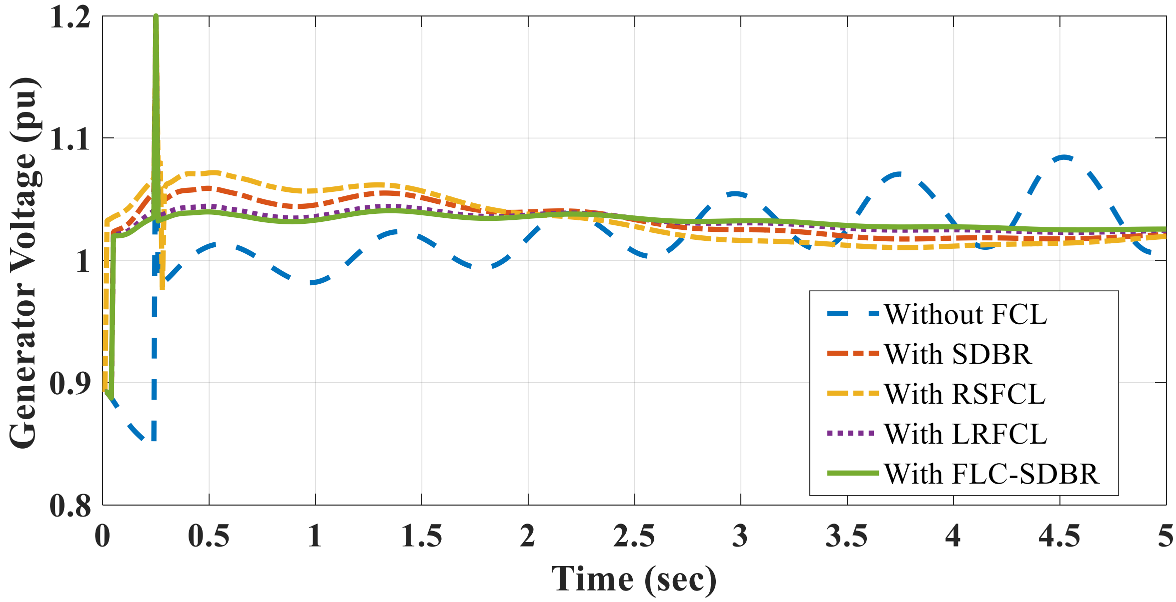

Fig 5. 11: DFIG terminal voltage for 0.5 pu dip in bus voltage

Fig 5. 12 and Fig 5. 13 show that output power drops to 0.7 pu and generator speed keeps increasing up to 414 rad/sec within 5 sec when the system is under 0.5 pu bus voltage for 250 ms. With the application of the FCL, both the quantities show small oscillations and return to a steady state after the clearance of the fault. Compared to other control strategies, FLC-SDBR performance is better.

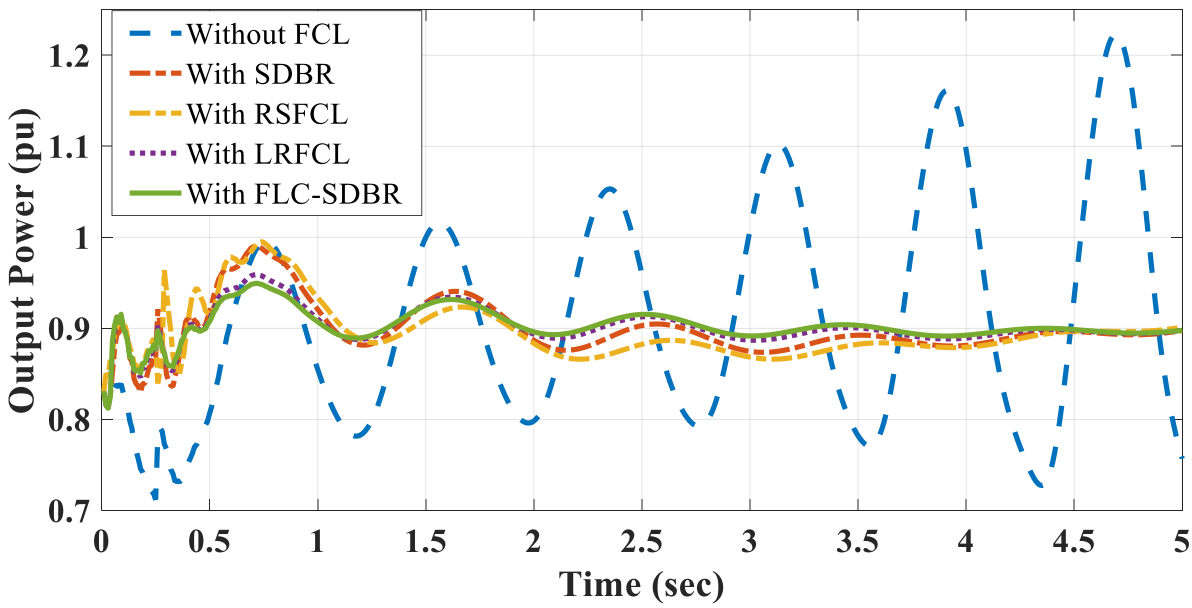

Fig 5. 12: DFIG output power for 0.5 pu dip in bus voltage

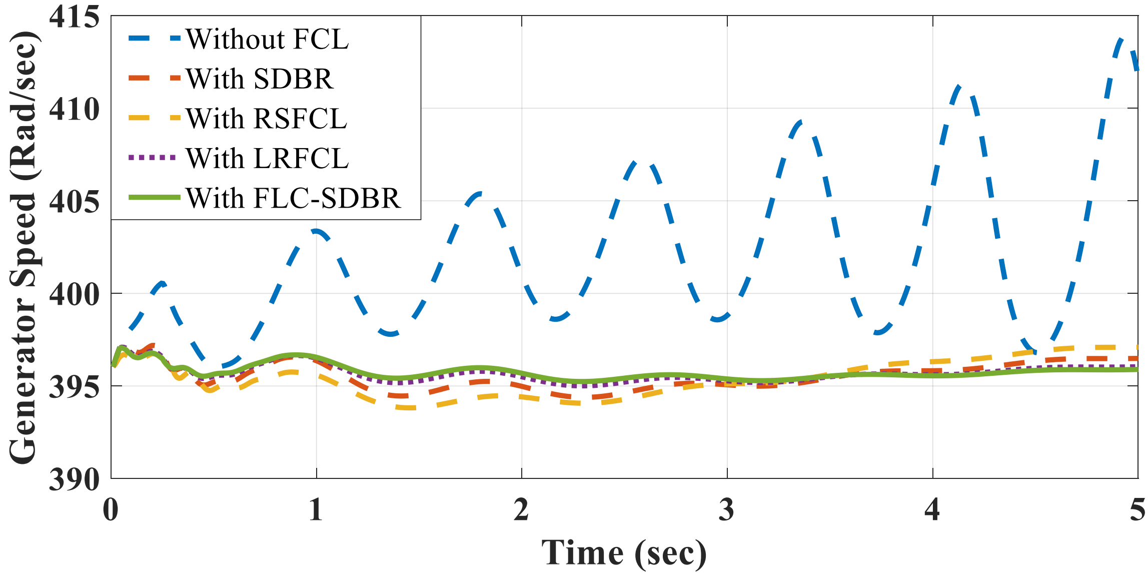

Fig 5. 13: DFIG rotor speed for 0.5 pu dip in bus voltage

5.2.3 Transient Stability Analysis for 0.75 pu Bus Voltage

The system is tested with 0.75 pu in bus voltage over a time period of 250 ms. Fig 5. 14 and Fig 5. 15 represent the stator and rotor current for the time period of 5 sec. Without the FCL, stator current rises to about 0.98 pu. With SDBR and RSFCL peak stator current is about 0.96 pu. Stator current is not being converged to the steady state value even after 5 sec of clearance of fault. This condition is due to the activation of a high value of resistance in series with DFIG in the case of less sag in bus voltage. With the application of LRFCL and FLC-SDBR, oscillation is low and stator current is near to the steady state value. With SDBR and RSFCL, the rotor current rises to about 1.1 pu. With LRFCL and FLC-SDBR, rotor current limits 0.97 pu and 0.95 pu respectively.

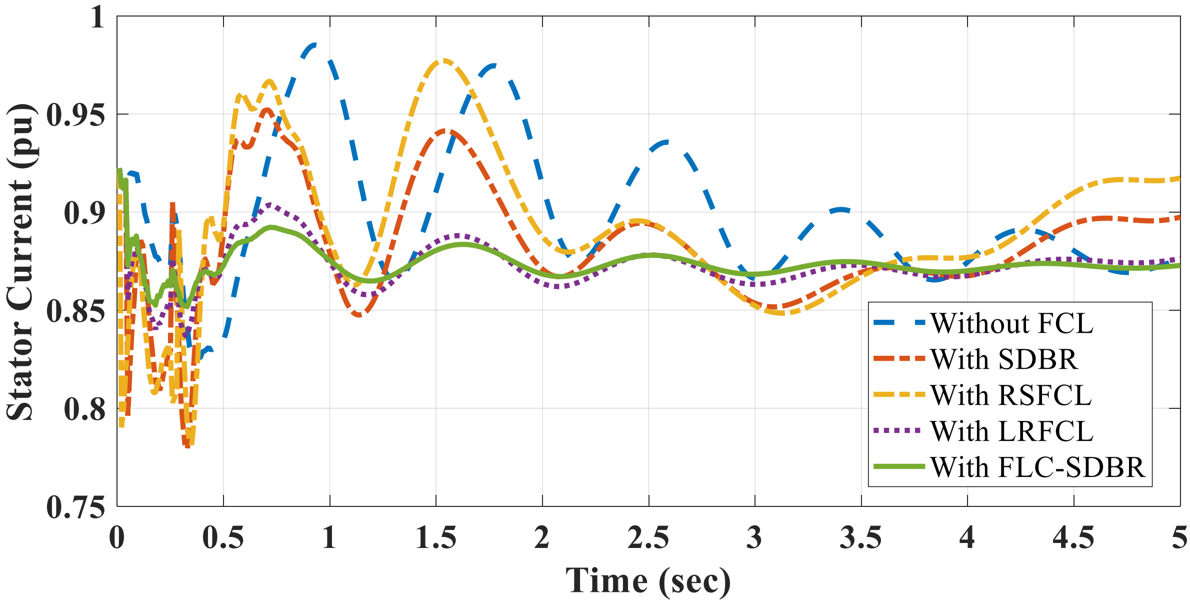

Fig 5. 14: Stator current for 0.75 pu dip in bus voltage

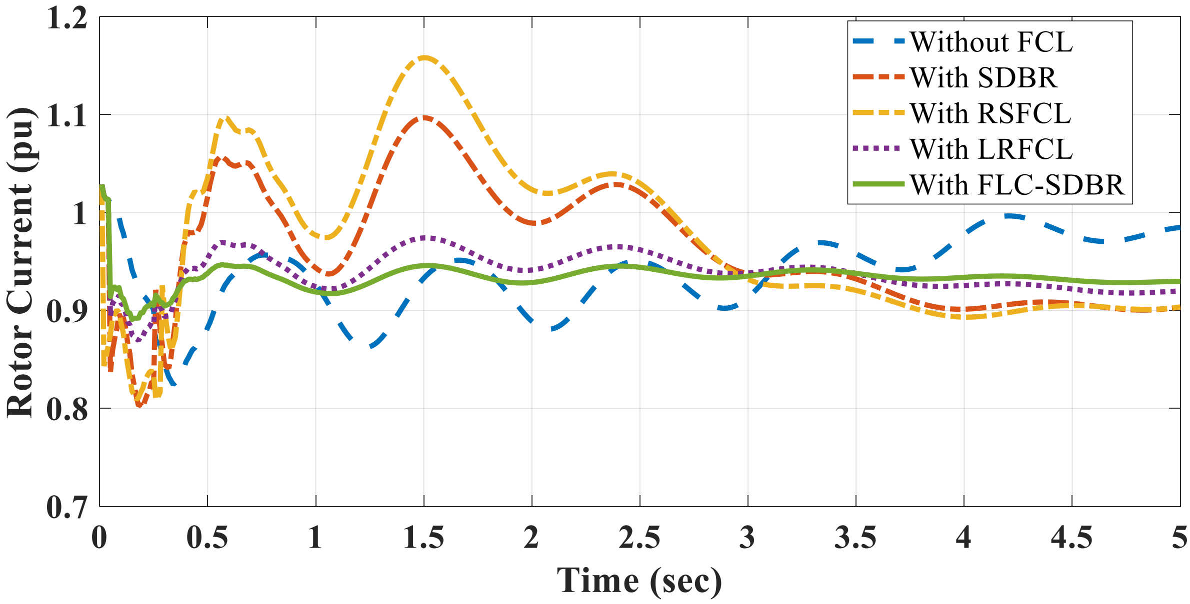

Fig 5. 15: Rotor current for 0.75 pu dip in bus voltage

Fig 5. 16 and Fig 5. 17 show the DC-link voltage and the terminal voltage of the DFIG respectively. Without the application of the FCL, the DC-link voltage falls below the steady state value (1 pu) and even after fault clearance it oscillates. With the application of the RSFCL and SDBR, the DC-link voltage increases to 1.07 pu and 1.06 pu respectively. Since the high amount of series resistance is triggered in the circuit to limit the fault current, DC-link voltage rises due to the failure of GSC to transfer adequate power to the grid. With the application of FLC-SDBR and LRFCL, only desirable resistance comes into effect, so the power transfer has been improved, which leads to the maintenance of the DC-link voltage. Also, for the terminal voltage similar kinds of phenomena can be observed. The terminal voltage response is better with the implementation of FLC-SDBR. From Fig 5. 18 and Fig 5. 19 we can see that the output power response and the rotor speed response has been improved with the application of the FLC-SDBR.

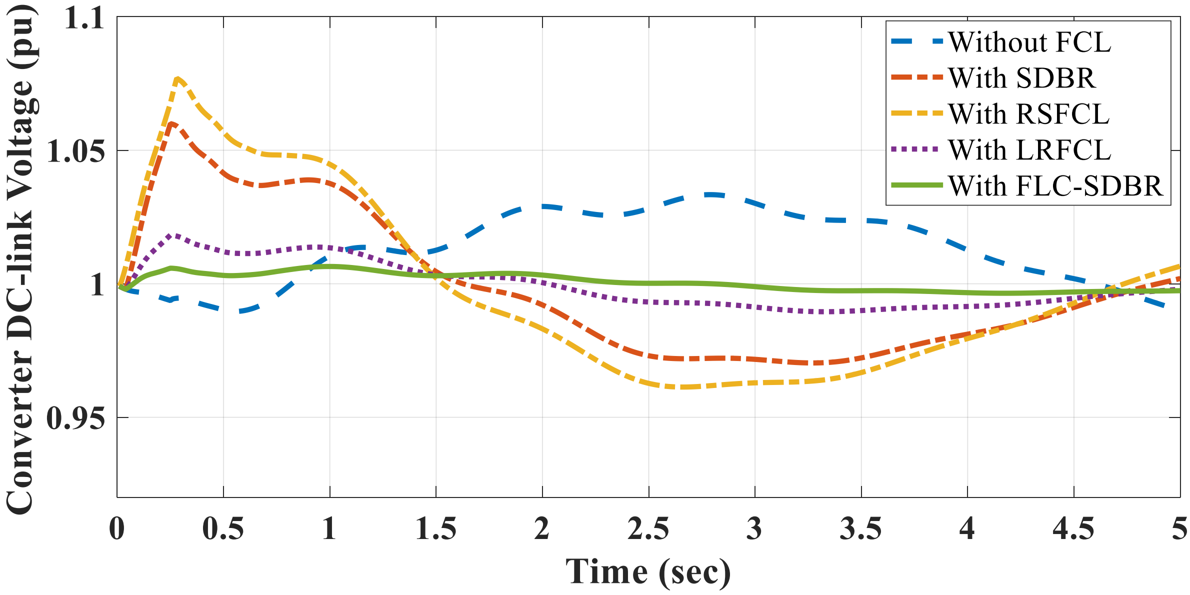

Fig 5. 16: Converter DC-link voltage for 0.75 pu dip in bus voltage

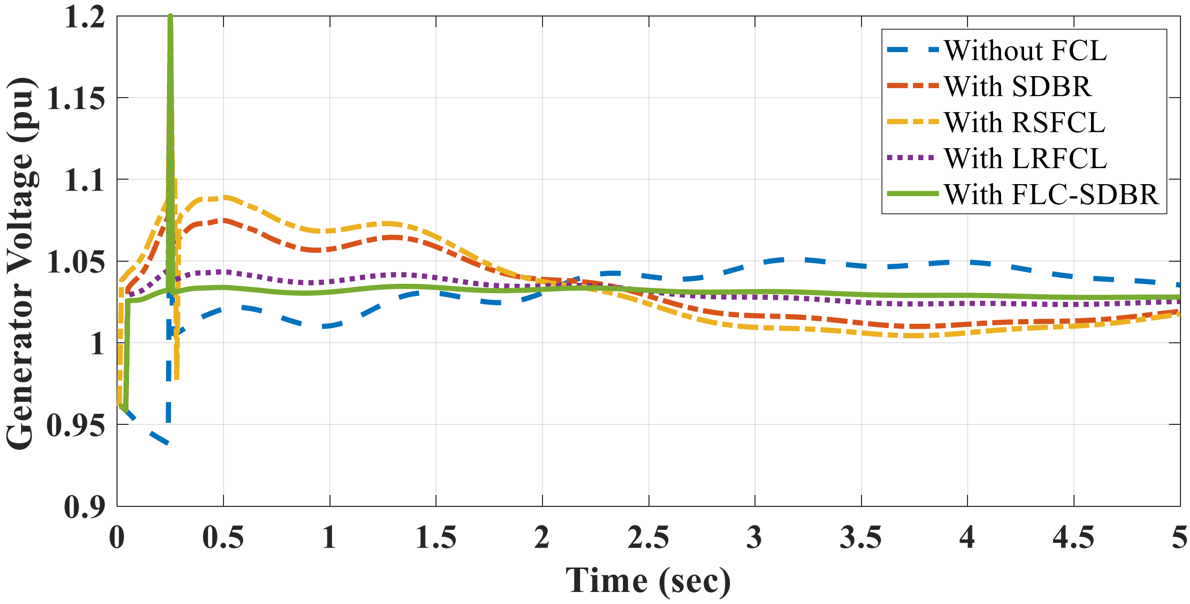

Fig 5. 17: DFIG terminal voltage for 0.75 pu dip in bus voltage

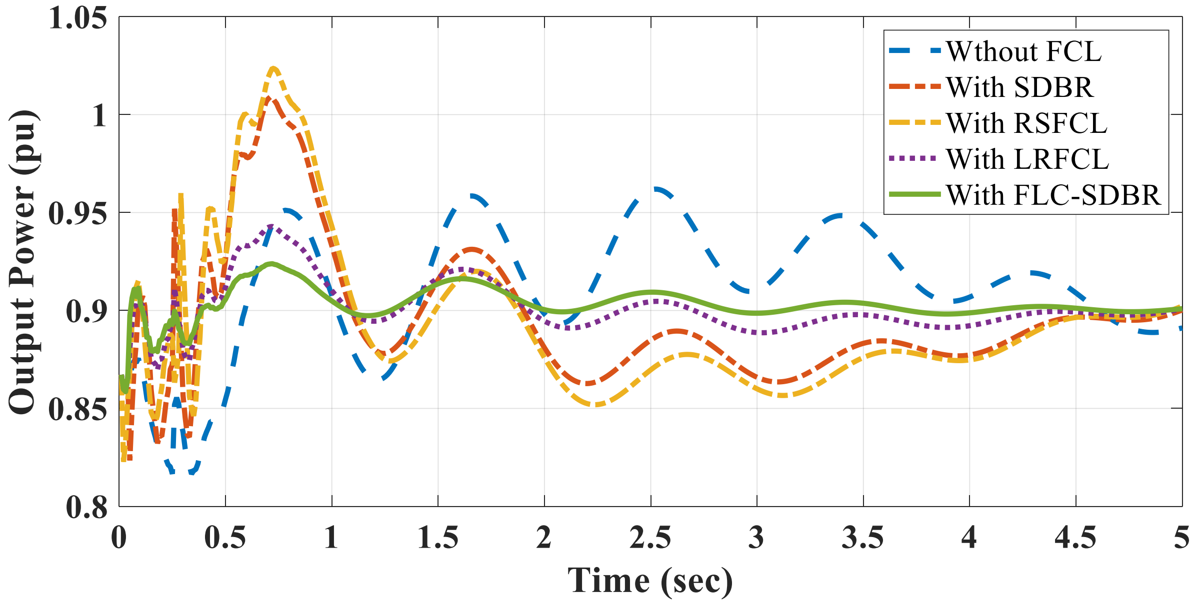

Fig 5. 18: DFIG output power for 0.75 pu dip in bus voltage

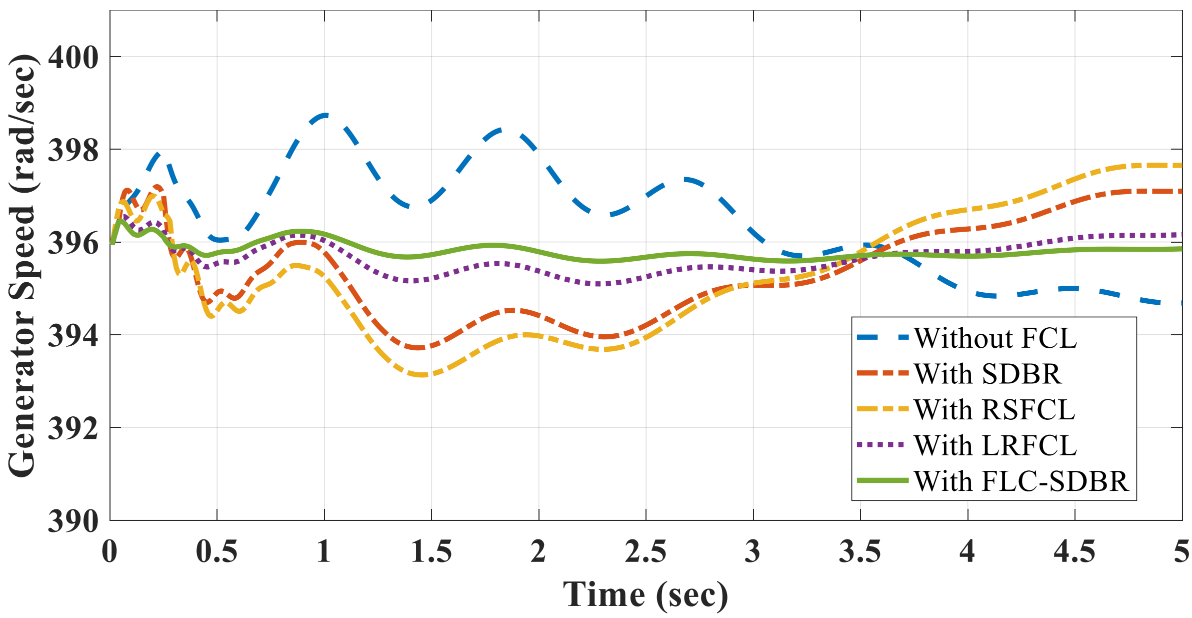

Fig 5. 19: DFIG rotor speed for 0.75 pu dip in bus voltage

5.3 Index Based Performance Analysis

The graphical analysis gives an overall view of the performance of FCL. An index-based performance analysis is conducted for a detailed and precise analysis of the different models [83, 31]. Several performance indices are calculated and compared to verify the effectiveness of the FCL and find the appropriate solution. This method provides the deviation from the steady state value. The lower value of the index means less deviation from the steady state thus, system performance is better. The various indices used are as follows.

Generator voltage deviation:

$$vlt(pu.s) = \int_0^T |\Delta V| \, dt \tag{5.1}$$

Stator current deviation:

$$str(pu.s) = \int_0^T |\Delta I_s| \, dt \tag{5.2}$$

Rotor current deviation:

$$rtr(pu.s) = \int_0^T |\Delta I_r| \, dt \tag{5.3}$$

Generator speed deviation:

$$spd(pu.s) = \int_0^T |\Delta \omega| \, dt \tag{5.4}$$

DC-link voltage deviation:

$$vdc(pu.s) = \int_0^T |\Delta V_{dc}| \, dt \tag{5.5}$$

Output power deviation:

$$pow(pu.s) = \int_0^T |\Delta P|\, dt \tag{5.6}$$

Here ΔV, ΔI_s, ΔI_r, $\Delta \omega$, ΔV_{dc}, and ΔP are the deviation in the generator terminal voltage, stator and rotor current, generator speed, DC-link voltage and active power from the steady state value. The absolute value of those quantity is taken. Deviation is calculated from 0 to 5 sec of simulation time. The indices value for 0 pu, 0.5 pu and 0.75 pu is presented in Table 3,Table 4 and Table 5 respectively.

Table 3: Performance indices for 0 pu bus voltage

Index Parameter (%)	Value of indices		
	No FCL	SDBR	RSFCL
Stator Current (pu.s)	462.43	11.08	4.36
Rotor Current (pu.s)	391.12	14.12	6.53
DC-link Voltage (pu.s)	36.65	5.13	2.7
Terminal Voltage (pu.s)	85.92	5.44	2.85
Output Power (pu.s)	228.61	9.76	4.9
Rotor Speed (pu.s)	78.12	0.95	0.33

Table 4: Performance indices for 0.5 pu bus voltage

Index Parameter (%)	Value of indices				
	No FCL	SDBR	RSFCL	LRFCL	FLC-SDBR
Stator Current (pu.s)	145.06	8.88	9.98	6.31	5.72
Rotor Current (pu.s)	94.44	18.98	25.72	10.66	8.71
DC-link Voltage (pu.s)	28.84	7.76	10.43	4.41	3.32
Terminal Voltage (pu.s)	14.72	7.06	9.65	4.04	3.22
Output Power (pu.s)	52.12	11.05	12.48	7.34	6.23
Rotor Speed (pu.s)	8.08	0.89	1.26	0.53	0.42

Table 5: Performance indices for 0.75 pu bus voltage

Index Parameter (%)	Value of indices				
	No FCL	SDBR	RSFCL	LRFCL	FLC-SDBR
Stator Current (pu.s)	15	11.27	15.72	3.99	2.56
Rotor Current (pu.s)	16.36	27.21	36.06	8.65	3.87
DC-link Voltage (pu.s)	8.06	10.91	13.99	3.8	1.46
Terminal Voltage (pu.s)	7.49	10.02	12.82	3.51	1.48
Output Power (pu.s)	13.37	13.74	15.91	5.25	2.81
Rotor Speed (pu.s)	1.45	1.3	1.71	0.45	0.19

From the above tables, it is observed that the values of performance indices are lower for the LRFCL and FLC-SDBR as compared to SDBR and RSFCL. Also, we can see that FLC-SDBR has the lowest indices value among all the control strategies. It can be concluded that the FLC-SDBR performance is better for any level of bus voltage sag.

For the practical implementation of the SDBR, a resistive dump load is needed. A large amount of power is needed to be absorbed in a short period of time during the fault. The practical implementation of large-sized dump loads in the range of 4 MW is suggested in a research paper [84]. They proposed the electrode boiler as a solution to dump load for massive power consumption during a brief period of power system failure. A large volume of liquid is heated inside the boiler and a large amount of active power is consumed. It is mentioned that the electrode boilers up to 50 MW are commercially available in an economical range. Hence electrode boilers can be used as the resistive load for the practical implementation of the proposed model.

Chapter 6

Conclusion and Future Work

6.1 Summary

A simulation model of the doubly fed induction generator (DFIG) along with its converter has been developed. All the basic components, like the aerodynamics model of a wind turbine, the drive train model, local load and the power grid, are modeled in MATLAB. There is a high penetration of wind power in the grid. DFIG needs to be in continuous operation during grid voltage sag for the time specified by the grid code. DFIG may get damaged due to overspeed of the generator rotor that occurs due to electrical and mechanical torque imbalance. The stator and rotor coil may burn out due to overheating caused by overcurrent. Surplus power during the voltage sag is needed to be absorbed in the dump load for the safe operation of DFIG from an electrical and mechanical point of view. The control systems to control the power flow in the dump load or series resistance are activated once the voltage falls below a certain threshold and its operation is identical for all levels of voltage sag.

It is known that in conventionally controlled series dynamic braking resistor (SDBR) and resistive-superconducting fault current limiter (RSFCL), there is no consideration of the different levels of voltage sag on the bus voltage for their activation. The system triggers a full resistance value once the faulty condition is encountered. The SDBR and RSFCL resistances are designed for the worst case of 0 pu bus voltage and the same value of resistance is applied to limit the fault current for any level of voltage dip in the bus voltage. Due to this, the system works perfectly for the worst-case scenario of 0 dip. But if the fault is less severe with a bus voltage of 0.5 pu or 0.75 pu it is observed that the proposed system did not work properly. The system is more unstable due to the addition of extra load in series on the grid side. Due to the overloading of DFIG, oscillation is high and system performance is worsened.

RSFCL needs no control action for its activation, so there is no risk of failure in the control system. But it will always be in series in transmission lines carrying a high amount of line current throughout its life, which is undesirable. SDBR is implemented in the system as FCL so that resistance will be triggered in the system only during the fault period. The IGBT switch will bypass resistive load during normal operating conditions. In this thesis work, ladder resistive fault current limiter (LRFCL) and fuzzy logic control-based series dynamic braking resistor (FLC-SDBR) have been proposed for low voltage ride through (LVRT) enhancement of DFIG. The performance of the proposed system is compared with that of conventional systems like SDBR and RSFCL.

6.2 Conclusions

LRFCL is proposed with the flexibility of triggering three different values of resistance in the system depending on the level of voltage sag. The resistance of SDBR designed for the worst-case scenario of 0 pu voltage sag is divided into two parts ($1/3^{rd}$ and $2/3^{rd}$). This resistance is triggered based on the bus voltage sag with the help of the IGBT switches and control circuit. The designed control system can sense and check the range of bus voltage sag. When the voltage falls within a specified range, its corresponding IGBT switching signal is triggered. It is observed that the LRFCL can enhance the system's overall transient stability for different levels of bus voltage sag.

FLC-SDBR is proposed, whose control action is more precise and effective than the LRFCL. In LRFCL, bus voltage sag is divided into different ranges and control action is taken based on that range of voltage change. But in the case of FLC-SDBR, control action changes for small incremental changes in bus voltage with the help of a fuzzy control scheme. Hence, a duty cycle is generated by sensing the change in bus voltage and a required effective resistance is triggered in the system. Observation shows that FLC-SDBR performance is superior to other control strategies in limiting the fault current, maintaining DC-link voltage, output power, and rotor speed. Simulation and numerical analysis, including index-based comparison show that FLC-SDBR stands superior for maintaining the system's stability. From the overall analysis, it can be concluded that FLC-SDBR is capable of enhancing the LVRT of DFIG for any level of sag in the bus voltage.

6.3 Future Work

Further study on the following issues can be taken up:

- The proposed control system model can be integrated with the microgrid system (PV, wind and Solar) and the impact of the system can be analyzed.
- Artificial intelligence-based techniques like adaptive network-based fuzzy inference system (ANFIS) and Artificial Neural Networks (ANNs) can be used for the generation of the control signal for SDBR.
- The proposed system can be implemented practically and tested to verify the practical feasibility of the developed system.
- Instead of using a single variable in a fuzzy system, multiple system variables like rotor current, stator current and rotor speed can be used for the generation of the control signal.

References

[1] "Wind Power – Analysis - IEA", *IEA*, 2022. [Online]. Available: https://www.iea.org/reports/wind-power. [Accessed: 12- May- 2022].

[2] "Wind energy", *European Commission - European Commission*, 2022. [Online]. Available:https://ec.europa.eu/info/research-and-innovation/research-area/energy-research-and-innovation/wind-energy_en. [Accessed: 12- May- 2022].

[3] "Wind energy in Europe: 2021 Statistics and the outlook for 2022-2026 | WindEurope", *WindEurope*, 2022. [Online]. Available: https://windeurope.org/intelligence-platform/product/wind-energy-in-europe-2021-statistics-and-the-outlook-for-2022-2026/. [Accessed: 12- May- 2022].

[4] "Global Wind Report 2021 - Global Wind Energy Council", *Global Wind Energy Council*, 2022. [Online]. Available: https://gwec.net/global-wind-report-2021/. [Accessed: 12- May- 2022].

[5] "Wind power", *AccessScience*. Available: 10.1036/1097-8542.746400 [Accessed 11 May 2022].

[6] A. Das, K. B. Chimonyo, T. R. Kumar, S. Gourishankar and C. Rani, "Vertical axis and horizontal axis wind turbine- A comprehensive review," *2017 International Conference on Energy, Communication, Data Analytics and Soft Computing (ICECDS)*, 2017, pp. 2660-2669, doi: 10.1109/ICECDS.2017.8389937.

[7] J. Bukala et al., "Small Wind Turbines: Specification, Design, and Economic Evaluation", *Wind Turbines - Design, Control and Applications*, 2016. Available: 10.5772/62821 [Accessed 11 May 2022].

[8] F. Castellani, D. Astolfi, M. Peppoloni, F. Natili, D. Buttà and A. Hirschl, "Experimental Vibration Analysis of a Small Scale Vertical Wind Energy System for Residential Use", *Machines*, vol. 7, no. 2, p. 35, 2019. Available: 10.3390/machines7020035 [Accessed 11 May 2022].

[9] A. Beainy, C. Maatouk, N. Moubayed and F. Kaddah, "Comparison of different types of generator for wind energy conversion system topologies," *2016 3rd International Conference on Renewable Energies for Developing Countries (REDEC)*, 2016, pp. 1-6, doi: 10.1109/REDEC.2016.7577535.

[10] A. E. Leon, M. F. Farias, P. E. Battaiotto, J. A. Solsona and M. I. Valla, "Control Strategy of a DVR to Improve Stability in Wind Farms Using Squirrel-Cage Induction Generators," *in IEEE Transactions on Power Systems*, vol. 26, no. 3, pp. 1609-1617, Aug. 2011, doi: 10.1109/TPWRS.2010.2088141.

[11] P. K. Goel, B. Singh, S. S. Murthy and N. Kishore, "Isolated Wind–Hydro Hybrid System Using Cage Generators and Battery Storage," *in IEEE Transactions on Industrial Electronics*, vol. 58, no. 4, pp. 1141-1153, April 2011, doi: 10.1109/TIE.2009.2037646.

[12] A. Uehara et al., "A Coordinated Control Method to Smooth Wind Power Fluctuations of a PMSG-Based WECS," *in IEEE Transactions on Energy Conversion*, vol. 26, no. 2, pp. 550-558, June 2011, doi: 10.1109/TEC.2011.2107912.

[13] M. E. Haque, M. Negnevitsky and K. M. Muttaqi, "A Novel Control Strategy for a Variable-Speed Wind Turbine With a Permanent-Magnet Synchronous Generator," *in IEEE Transactions on Industry Applications*, vol. 46, no. 1, pp. 331-339, Jan.-feb. 2010, doi: 10.1109/TIA.2009.2036550.

[14] A. Radaideh, M. Bodoor and A. Al-Quraan, "Active and Reactive Power Control for Wind Turbines Based DFIG Using LQR Controller with Optimal Gain-Scheduling", *Journal of Electrical and Computer Engineering*, vol. 2021, pp. 1-19, 2021. Available: 10.1155/2021/1218236 .

[15] S. Muller, M. Deicke and R. W. De Doncker, "Doubly fed induction generator systems for wind turbines," *in IEEE Industry Applications Magazine*, vol. 8, no. 3, pp. 26-33, May-June 2002, doi: 10.1109/2943.999610.

[16] J. Morren and S. W. H. de Haan, "Ride through of wind turbines with doubly-fed induction generator during a voltage dip," *in IEEE Transactions on Energy Conversion*, vol. 20, no. 2, pp. 435-441, June 2005, doi: 10.1109/TEC.2005.845526.

[17] A. Dida and D. Benattous, "Doubly-Fed Induction Generator Drive System Based on Maximum Power Curve Searching using Fuzzy Logic Controller", *International Journal of Power Electronics and Drive Systems (IJPEDS)*, vol. 5, no. 4, p. 583, 2015. Available: 10.11591/ijpeds.v5.i4.pp583-594.

[18] Wei Qiao and R. Harley, "Grid Connection Requirements and Solutions for DFIG Wind Turbines", *2008 IEEE Energy 2030 Conference*, 2008. Available: 10.1109/energy.2008.4781068.

[19] A. Arulampalam, G. Ramtharan, N. Jenkins, V. K. Ramachandaramurthy, J. B. Ekanayake and G. Strbac, "Trends in wind power technology and grid code requirements," *2007 International Conference on Industrial and Information Systems*, 2007, pp. 129-134, doi: 10.1109/ICIINFS.2007.4579161.

[20] M. Nadour, A. Essadki and T. Nasser, "Improving low-voltage ride-through capability of a multimegawatt DFIG based wind turbine under grid faults", *Protection and Control of Modern Power Systems*, vol. 5, no. 1, 2020. Available: 10.1186/s41601-020-00172-w [Accessed 12 May 2022].

[21] B. E. Elnaghi, M. E. Dessouki and F. A. Elkader, "Experimental investigation of pitch angle controller for DFIG based wind energy conversion system," *2017 Nineteenth International Middle East Power Systems Conference (MEPCON)*, 2017, pp. 1477-1482, doi: 10.1109/MEPCON.2017.8301378.

[22] A. Kadri, H. Marzougui and F. Bacha, "MPPT control methods in wind energy conversion system using DFIG," *2016 4th International Conference on Control Engineering & Information Technology (CEIT)*, 2016, pp. 1-6, doi: 10.1109/CEIT.2016.7929115.

[23] M. A. H. Soliman, H. Soliman and P. K. Soori, "Analysis of the dynamic behavior and LVRT capability of a DFIG using SDBR during grid disturbances," *2013 7th IEEE GCC Conference and Exhibition (GCC)*, 2013, pp. 436-439, doi: 10.1109/IEEEGCC.2013.6705818.

[24] M. R. Islam et al., "Enhancement of FRT Capability of DFIG Based Wind Farm by a Hybrid Superconducting Fault Current Limiter With Bias Magnetic Field," *2020 IEEE International Conference on Power Electronics, Smart Grid and Renewable Energy (PESGRE2020)*, 2020, pp. 1-6, doi: 10.1109/PESGRE45664.2020.9070632.

[25] M. R. Islam, J. Hasan, M. N. Huda and M. A. H. Sadi, "Fault Ride Through Capability Improvement of DFIG Based Wind Farms Using Active Power Controlled Bridge Type

Fault Current Limiter," *2019 North American Power Symposium (NAPS)*, 2019, pp. 1-6, doi: 10.1109/NAPS46351.2019.9000292.

[26] M. E. Hossain, "Performance of new solid-state fault current limiter for transient stability enhancement of DFIG based wind generator," *2017 North American Power Symposium (NAPS)*, 2017, pp. 1-6, doi: 10.1109/NAPS.2017.8107187.

[27] A. Mokarim, B. Dwivedi and P. Verma, "Comparative study of different Bridge Fault Current Limiters applied in Doubly Fed Induction Generator for Improvement of Fault Ride-Through Capability," *2019 International Conference on Automation, Computational and Technology Management (ICACTM)*, 2019, pp. 256-261, doi: 10.1109/ICACTM.2019.8776771.

[28] M. E. Hossain, "Transient stability improvement analysis among the series fault current limiters for DFIG based wind generator," *2017 19th International Conference on Intelligent System Application to Power Systems (ISAP),* 2017, pp. 1-6, doi: 10.1109/ISAP.2017.8071373.

[29] M. R. Islam, J. Hasan, M. R. Islam, A. Z. Kouzani and M. A. Parvez Mahmud, "Optimized Use of Flux Coupling Superconducting Fault Current Limiter to Improve the Performance of DFIG Based Wind Power Generation System," *2020 IEEE International Conference on Applied Superconductivity and Electromagnetic Devices (ASEMD)*, 2020, pp. 1-2, doi: 10.1109/ASEMD49065.2020.9276093.

[30] G. Rashid and M. H. Ali, "Nonlinear Control-Based Modified BFCL for LVRT Capacity Enhancement of DFIG-Based Wind Farm," *in IEEE Transactions on Energy Conversion*, vol. 32, no. 1, pp. 284-295, March 2017, doi: 10.1109/TEC.2016.2603967.

[31] G. Rashid and M. H. Ali, “Fault ride through capability improvement of DFIG based wind farm by Fuzzy Logic controlled parallel resonance fault current limiter,” *Electric Power Systems Research*, vol. 146, pp. 1–8, 2017.

[32] M. R. Islam, J. Hasan, M. R. R. Shipon, M. A. H. Sadi, A. Abuhussein and T. K. Roy, "Neuro Fuzzy Logic Controlled Parallel Resonance Type Fault Current Limiter to Improve the Fault Ride Through Capability of DFIG Based Wind Farm," *in IEEE Access*, vol. 8, pp. 115314-115334, 2020, doi: 10.1109/ACCESS.2020.3000462.

[33] S. Yang, T. Zhou, X. Zhen, X. Zhang, R. Shao and L. Chang,” A SCR crowbar commutated with rotor-side converter for doubly fed wind turbines,” *2015 IEEE 6th International Symposium on Power Electronics for Distributed Generation Systems (PEDG)*, 2015, pp. 1-7, doi: 10.1109/PEDG.2015.7223084.

[34] L. G. Meegahapola, T. Littler and D. Flynn,” Decoupled-DFIG Fault Ride-Through Strategy for Enhanced Stability Performance During Grid Faults,” *in IEEE Transactions on Sustainable Energy*, vol. 1, no. 3, pp. 152-162, Oct. 2010, doi: 10.1109/TSTE.2010.2058133.

[35] J. Han, W. Jia, Y. Wang, L. Zhou, H. Hu and Y. Ren,” An Optimized Strategy of Switching Crowbar Improve LVRT of DFIG Based on RTDS,” *2020 IEEE Sustainable Power and Energy Conference (iSPEC)*, 2020, pp. 775-780, doi: 10.1109/iSPEC50848.2020.9351162.

[36] L. Shi, N. Chen and Q. Lu, "Dynamic Characteristic Analysis of Doubly-fed Induction Generator Low Voltage Ride-through", *Energy Procedia*, vol. 16, pp. 1526-1534, 2012. Available: 10.1016/j.egypro.2012.01.239

[37] J. Li, Q. Qiu and M. Zhan," An Improved Crowbar Control Circuit of DFIG during LVRT," *2021 IEEE 4th International Electrical and Energy Conference (CIEEC),* 2021, pp. 1-6, doi: 10.1109/CIEEC50170.2021.9510598.

[38] C. He, Q. Tan, N. Zhang, J. Chen, R. Shen and X. Wu," Research on Low Voltage Ride Through Capability of DFIG Based on Adaptive Crowbar Resistor," *2018 37th Chinese Control Conference (CCC),* 2018, pp. 8930-8935, doi: 10.23919/ChiCC.2018.8482616.

[39] K. E. Okedu, S. M. Muyeen, R. Takahashi and J. Tamura," Application of SDBR with DFIG to augment wind farm fault ride through*," 2011 International Conference on Electrical Machines and Systems*, 2011, pp. 1-6, doi: 10.1109/ICEMS.2011.6073472.

[40] A. Causebrook, D. J. Atkinson and A. G. Jack," Fault Ride-Through of Large Wind Farms Using Series Dynamic Braking Resistors (March 2007)," *in IEEE Transactions on Power Systems*, vol. 22, no. 3, pp. 966975, Aug. 2007, doi: 10.1109/TPWRS.2007.901658.

[41] H. Soliman, H. Wang, D. Zhou, F. Blaabjerg and M. I. Marie," Sizing of the series dynamic breaking resistor in a doubly fed induction generator wind turbine," *2014 IEEE Energy Conversion Congress and Exposition (ECCE)*, 2014, pp. 1842-1846, doi: 10.1109/ECCE.2014.6953642.

[42] K. E. Okedu," Optimal position and best switching signal of SDBR in DFIG wind turbine low voltage ride through low voltage ride through capability of Doubly Fed Induction Generators," *2017 IEEE International Electric Machines and Drives Conference (IEMDC),* 2017, pp. 1-6, doi: 10.1109/IEMDC.2017.8001868.

[43] K. E. Okedu, S. M. Muyeen, R. Takahashi and J. Tamura," Comparative study between two protection schemes for DFIG-based wind generator," *2010 International Conference on Electrical Machines and Systems*, 2010, pp. 62-67.

[44] G. Pannell, B. Zahawi, D. J. Atkinson and P. Missailidis," Evaluation of the Performance of a DC-Link Brake Chopper as a DFIG Low-Voltage Fault-Ride-Through Device," *in IEEE Transactions on Energy Conversion*, vol. 28, no. 3, pp. 535-542, Sept. 2013, doi: 10.1109/TEC.2013.2261301.

[45] K. E. Okedu, S. M. Muyeen, R. Takahashi and J. Tamura," Protection schemes for DFIG considering rotor current and DC-link voltage," *2011 International Conference on Electrical Machines and Systems*, 2011, pp. 1-6, doi: 10.1109/ICEMS.2011.6073453.

[46] S. Behzad Naderi, M. Negnevitsky and K. M. Muttaqi," A modified DC chopper for limiting the fault current and controlling the DC link voltage to enhance ride-through capability of doubly-fed induction generator based wind turbine," *2017 IEEE Industry Applications Society Annual Meeting, 2017*, pp. 1-8, doi: 10.1109/IAS.2017.8101743.

[47] O. Noureldeen and I. Hamdan," Design and Analysis of Combined Chopper-Crowbar Protection Scheme for Wind Power System Based on Artificial Intelligence," *2018 Twentieth International Middle East Power Systems Conference (MEPCON)*, 2018, pp. 809-814, doi: 10.1109/MEPCON.2018.8635177.

[48] Z. -C. Zou, Z. -L. Mu, R. Ou, Y. Lei, H. -B. Li and K. -T. Jiang," Improving Dynamic Performance of DFIG Using Rotor-Side SFCL and DCLink Brake Chopper During Grid Voltage Swell," *2020 IEEE International Conference on Applied Superconductivity and Electromagnetic Devices (ASEMD)*, 2020, pp. 1-2, doi: 10.1109/ASEMD49065.2020.9276126.

[49] W. Guo, L. Xiao and S. Dai," Enhancing Low-Voltage Ride-ThroughCapability and Smoothing Output Power of DFIG With a Superconducting Fault-Current Limiter–Magnetic Energy Storage System," *in IEEE Transactions on Energy Conversion*, vol. 27, no. 2, pp. 277-295, June 2012, doi: 10.1109/TEC.2012.2187654.

[50] Y. Shen, D. Ke, W. Qiao, Y. Sun, D. S. Kirschen and C. Wei," Transient Reconfiguration and Coordinated Control for Power Converters to Enhance the LVRT of a DFIG Wind Turbine With an Energy Storage Device," *in IEEE Transactions on Energy Conversion*, vol. 30, no. 4, pp. 1679-1690, Dec. 2015, doi: 10.1109/TEC.2015.2449900.

[51] Y. Shen, D. Ke, Y. Sun, D. S. Kirschen, W. Qiao and X. Deng," Advanced Auxiliary Control of an Energy Storage Device for Transient Voltage Support of a Doubly Fed Induction Generator," *in IEEE Transactions on Sustainable Energy*, vol. 7, no. 1, pp. 63-76, Jan. 2016, doi: 10.1109/TSTE.2015.2472299.

[52] X. Xiao, R. Yang, Z. Zheng and Y. Wang," Cooperative Rotor-Side SMES and Transient Control for Improving the LVRT Capability of Grid-Connected DFIG-Based Wind Farm," *in IEEE Transactions on Applied Superconductivity*, vol. 29, no. 2, pp. 1-5, March 2019, Art no. 0600204, doi: 10.1109/TASC.2018.2881315.

[53] Chi Jin and Peng Wang," Enhancement of low voltage ride-through capability for wind turbine driven DFIG with active crowbar and battery energy storage system," *IEEE PES General Meeting*, 2010, pp. 1-8, doi: 10.1109/PES.2010.5588180.

[54] N. S. Gayathri and N. Senroy," Wind turbine with flywheel for improved power smoothening and LVRT," *2013 IEEE Power Energy Society General Meeting*, 2013, pp. 1-5, doi: 10.1109/PESMG.2013.6672812.

[55] M. E. Elshiekh, D. -E. A. Mansour and A. M. Azmy," Improving Fault Ride-Through Capability of DFIG-Based Wind Turbine Using Superconducting Fault Current Limiter," *in IEEE Transactions on Applied Superconductivity*, vol. 23, no. 3, pp. 5601204-5601204, June 2013, Art no. 5601204, doi: 10.1109/TASC.2012.2235132.

[56] Z. -C. Zou, X. -Y. Xiao, Y. -F. Liu, Y. Zhang and Y. -H. Wang," Integrated Protection of DFIG-Based Wind Turbine With a Resistive-Type SFCL Under Symmetrical and

Asymmetrical Faults," *in IEEE Transactions on Applied Superconductivity*, vol. 26, no. 7, pp. 1-5, Oct. 2016, Art no. 5603005, doi: 10.1109/TASC.2016.2574352.

[57] K. -J. Du, X. -Y. Xiao, Y. Wang, Z. -X. Zheng and C. -S. Li," Enhancing Fault Ride-Through Capability of DFIG-Based Wind Turbines Using Inductive SFCL With Coordinated Control," *in IEEE Transactions on Applied Superconductivity*, vol. 29, no. 2, pp. 1-6, March 2019, Art no. 5400506, doi: 10.1109/TASC.2018.2883797.

[58] L. Chen, H. Chen, Z. Shu, G. Zhang, T. Xia and L. Ren," Comparison of Inductive and Resistive SFCL to Robustness Improvement of a VSCHVDC System With Wind Plants Against DC Fault*," in IEEE Transactions on Applied Superconductivity*, vol. 26, no. 7, pp. 1-8, Oct. 2016, Art no.5603508, doi: 10.1109/TASC.2016.2595622.

[59] M. Hossain and H. Ali," Asymmetric fault ride through capability enhancement of DFIG based variable speed wind generator by DC resistive fault current limiter," *2016 IEEE/PES Transmission and Distribution Conference and Exposition (TD)*, 2016, pp. 1-5, doi: 10.1109/TDC.2016.7519865.

[60] J. Hasan, M. R. Islam, M. R. Islam, A. Z. Kouzani and M. A. P. Mahmud," A Capacitive Bridge-Type Superconducting Fault Current Limiter to Improve the Transient Performance of DFIG/PV/SG-Based Hybrid Power System," *in IEEE Transactions on Applied Superconductivity*, vol. 31, no.8, pp. 1-5, Nov. 2021, Art no. 5603605, doi: 10.1109/TASC.2021.3094422.

[61] K. -J. Du, X. -P. Ma, Z. -X. Zheng, C. -S. Li, W. -X. Hu and K. -S. Dong," LVRT Capability Improvement of DFIG-Based Wind Turbines With a Modified Bridge-Resistive-Type SFCL," *in IEEE Transactions on Applied Superconductivity*, vol. 31, no. 8, pp. 1-5, Nov. 2021, Art no. 5603005, doi: 10.1109/TASC.2021.3091114.

[62] L. Chen, C. Deng, F. Zheng, S. Li, Y. Liu and Y. Liao," Fault Ride-Through Capability Enhancement of DFIG-Based Wind Turbine With a Flux-Coupling-Type SFCL Employed at Different Locations," *in IEEE Transactions on Applied Superconductivity*, vol. 25, no. 3, pp. 1-5, June 2015, Art no. 5201505, doi: 10.1109/TASC.2014.2373511.

[63] L. Chen, F. Zheng, C. Deng, Z. Li and F. Guo," Fault Ride-Through Capability Improvement of DFIG-Based Wind Turbine by Employing a Voltage-Compensation-Type Active SFCL," *in Canadian Journal of Electrical and Computer Engineering*, vol. 38, no. 2, pp. 132-142, Spring 2015, doi: 10.1109/CJECE.2015.2406665.

[64] I. Ngamroo and T. Karaipoom," Cooperative Control of SFCL and SMES for Enhancing Fault Ride Through Capability and Smoothing Power Fluctuation of DFIG Wind Farm," *in IEEE Transactions on Applied Superconductivity*, vol. 24, no. 5, pp. 1-4, Oct. 2014, Art no. 5400304, doi: 10.1109/TASC.2014.2340445.

[65] R. Ou, X. -Y. Xiao, Z. -C. Zou, Y. Zhang and Y. -H. Wang," Cooperative Control of SFCL and Reactive Power for Improving the Transient Voltage Stability of Grid-Connected Wind Farm With DFIGs," *in IEEE Transactions on Applied Superconductivity*, vol. 26, no. 7, pp. 1-6, Oct. 2016, Art no. 5402606, doi: 10.1109/TASC.2016.2574344.

[66] G. Rashid and M. Hasan Ali," Bridge-type fault current limiter for asymmetric fault ride-through capacity enhancement of doubly fed induction machine based wind generator," *2014 IEEE Energy Conversion Congress and Exposition (ECCE)*, 2014, pp. 1903-1910, doi: 10.1109/ECCE.2014.6953651.

[67] U. Chaudhary, P. Tripathy and S. K. Nayak," Application of bridge-type FCL for betterment of FRT capability for DFIG-based wind turbine," *2014 6th IEEE Power India*

International Conference (PIICON), 2014, pp. 1-6, doi: 10.1109/POWERI.2014.7117687.

[68] M. Firouzi and G. B. Gharehpetian,” LVRT Performance Enhancement of DFIG-Based Wind Farms by Capacitive Bridge-Type Fault Current Limiter,” *in IEEE Transactions on Sustainable Energy*, vol. 9, no. 3, pp. 1118-1125, July 2018, doi: 10.1109/TSTE.2017.2771321.

[69] G. Rashid and M. H. Ali,” Asymmetrical fault ride through capacity augmentation of DFIG based wind farms by parallel resonance fault current limiter,” *2016 IEEE Power and Energy Society General Meeting (PESGM)*, 2016, pp. 1-5, doi: 10.1109/PESGM.2016.7741506.

[70] G. Abad, J. Lopez, M.A. Rodríguez, et al. (2011) Doubly Fed InductionMachine:Modeling and Control forWind Energy Generation, John Wiley & Sons, Inc.

[71] E. S. Abdin and W. Xu, "Control design and dynamic performance analysis of a wind turbine-induction generator unit," *in IEEE Transactions on Energy Conversion*, vol. 15, no. 1, pp. 91-96, March 2000, doi: 10.1109/60.849122.

[72] S. Heier, *Grid integration of wind energy conversion systems*, Second Edition (New York: John Wiley & Sons Ltd., 2007)

[73] A. H. M. A. Rahim and E. P. Nowicki, “Supercapacitor Energy Storage System for fault ride-through of a DFIG wind generation system,” *Energy Conversion and Management*, vol. 59, pp. 96–102, 2012.

[74] A. H. M. A. Rahim and I. O. Habiballah, “DFIG rotor voltage control for system dynamic performance enhancement,” *Electric Power Systems Research*, vol. 81, no. 2, pp. 503–509, 2011.

[75] A. H. M. A. Rahim, I. O. Habiballah, and E. P. Nowicki, “Identification and verification of hierarchy of DFIG converter controls for power system damping,” *International Journal of Modelling and Simulation*, vol. 31, no. 2, 2011.

[76] A. H. M. A. Rahim and E. P. Nowicki, “Modelling of doubly fed induction generator in a multimachine AC system with smes control,” *International Journal of Modelling and Simulation*, vol. 33, no. 2, 2013.

[77] G. Rashid and M. H. Ali, "Transient Stability Enhancement of Doubly Fed Induction Machine-Based Wind Generator by Bridge-Type Fault Current Limiter," *in IEEE Transactions on Energy Conversion*, vol. 30, no. 3, pp. 939-947, Sept. 2015, doi: 10.1109/TEC.2015.2400220.

[78] M. Firouzi, M. Nasiri, M. Benbouzid, and G. B. Gharehpetian, “Application of multi-step bridge-type fault current Limiter for Fault ride-through capability enhancement of permanent magnet synchronous generator-based wind turbines,” *International Transactions on Electrical Energy Systems*, vol. 30, no. 11, 2020.

[79] J. Moon, S. Lim, J. Kim and S. Yun,” Assessment of the Impact of SFCL on Voltage Sags in Power Distribution System,” *in IEEE Transactions on Applied Superconductivity*, vol. 21, no. 3, pp. 2161-2164, June 2011, doi: 10.1109/TASC.2010.2093592.

[80] J. Moon and J. Kim,” Voltage Sag Analysis in Loop Power Distribution System With SFCL,” *in IEEE Transactions on Applied Superconductivity*, vol. 23, no. 3, pp. 5601504-5601504, June 2013, Art no. 5601504, doi: 10.1109/TASC.2013.2238374.

[81] F. Topaloğlu and H. Pehlıvan, "Comparison of Mamdani type and Sugeno type fuzzy inference systems in wind power plant installations," 2018 6th International Symposium

on Digital Forensic and Security (ISDFS), 2018, pp. 1-4, doi: 10.1109/ISDFS.2018.8355384.

[82] S. A D, M. R. lingam, and B. A. radha, “A comprehensive study on fuzzy inference system and its application in the field of engineering,” *International Journal of Engineering Trends and Technology*, vol. 54, no. 1, pp. 36–40, 2017.

[83] G. Rashid and M. H. Ali,” Transient Stability Enhancement of Doubly Fed Induction Machine-Based Wind Generator by Bridge-Type Fault Current Limiter,” *in IEEE Transactions on Energy Conversion*, vol. 30, no. 3, pp. 939-947, Sept. 2015, doi: 10.1109/TEC.2015.2400220.

[84] U. Lundin and J. Bladh, "Demonstration of a Dynamic Braking System for Reduced Runaway Speed of Hydraulic Turbines", *Journal of Power and Energy Engineering*, vol. 05, no. 12, pp. 46-57, 2017. Available: 10.4236/jpee.2017.512007 [Accessed 27 June 2022].

Appendix A.

The parameter values of the DFIG are in per unit, except stated otherwise.

R_s	Stator resistance	0.0049
x_s	Stator reactance	4.0462
R_r	Rotor resistance	0.0059
x_r	Rotor reactance	4.1538
x_m	Stator-rotor mutual reactance	3.9538
R_a	Stator side converter resistance	0.001
X_a	Stator side converter reactance	0.1
C	Converter capacitance	1
R	Transmission line resistance	0.05
X	Transmission line reactance	0.2
H_g	Inertia constant of generator	0.5 s
H_t	Inertia constant of turbine	3 s
g_{11}	Conductance of local load	0.403
b_{11}	Susceptance of local load	0.1014
ρ	Air density	1.225 kg/m^3
A	Area swept by turbine blade	577 m^2
V_w	Wind velocity	12 m/s
D_g	Damping coefficient of generator	0
D_t	Damping coefficient of turbine	0
	Blade radius	13.5 m
	Gear ratio	100

Appendix B.

The parameter values of the Superconducting fault current limiter are:

t_0	Time to start quenching	10ms
t_1	1^{st} recovery time	0.25 sec
t_2	2^{nd} recovery time	0.28 sec
t_3	Complete recovery time	0.3 sec
R_m	Maximum resistance of RSFCL	2.1356 pu
Constant	a1	-35
	a2	-41
	b1	R_m
	b2	$R_m/2$